

# The Primordial Binary Population

## I: A near-infrared adaptive optics search for close visual companions to A star members of Scorpius OB2

M.B.N. Kouwenhoven<sup>1</sup>, A.G.A. Brown<sup>2</sup>, H. Zinnecker<sup>3</sup>, L. Kaper<sup>1</sup>, and S.F. Portegies Zwart<sup>1,4</sup>

<sup>1</sup> Astronomical Institute ‘Anton Pannekoek’, University of Amsterdam, Kruislaan 403, 1098 SJ Amsterdam, The Netherlands  
e-mail: kouwenho@science.uva.nl, lexk@science.uva.nl

<sup>2</sup> Leiden Observatory, University of Leiden, P.O. Box 9513, 2300 RA Leiden, The Netherlands  
e-mail: brown@strw.leidenuniv.nl

<sup>3</sup> Astrophysikalisches Institut Potsdam, An der Sternwarte 16, D-1 4482, Potsdam, Germany e-mail: hzinnecker@aip.de

<sup>4</sup> Section Computer Science, University of Amsterdam, Kruislaan 403, 1098 SJ Amsterdam, The Netherlands  
e-mail: spz@science.uva.nl

Received October 28, 2018; accepted October 28, 2018

**Abstract.** We present the results of a near-infrared adaptive optics survey with the aim to detect close companions to *Hipparcos* members in the three subgroups of the nearby OB association Sco OB2: Upper Scorpius (US), Upper Centaurus Lupus (UCL) and Lower Centaurus Crux (LCC). We have targeted 199 A-type and late B-type stars in the  $K_S$  band, and a subset also in the  $J$  and  $H$  band. We find 151 stellar components other than the target stars. A brightness criterion is used to separate these components into 77 background stars and 74 candidate physical companion stars. Out of these 74 candidate companions, 41 have not been reported before (14 in US; 13 in UCL; 14 in LCC). The angular separation between primaries and observed companion stars ranges from 0.22'' to 12.4''. At the mean distance of Sco OB2 (130 pc) this corresponds to a projected separation of 28.6 AU to 1612 AU. Absolute magnitudes are derived for all primaries and observed companions using the parallax and interstellar extinction for each star individually. For each object we derive the mass from  $K_S$ , assuming an age of 5 Myr for the US subgroup, and 20 Myr for the UCL and LCC subgroups. Companion star masses range from 0.10  $M_\odot$  to 3.0  $M_\odot$ . The mass ratio distribution follows  $f(q) = q^{-\Gamma}$  with  $\Gamma = 0.33$ , which excludes random pairing. No close ( $\rho \leq 3.75''$ ) companion stars or background stars are found in the magnitude range  $12 \text{ mag} \leq K_S \leq 14 \text{ mag}$ . The lack of stars with these properties cannot be explained by low-number statistics, and may imply a lower limit on the companion mass of  $\sim 0.1 M_\odot$ . Close stellar components with  $K_S > 14 \text{ mag}$  are observed. If these components are very low-mass companion stars, a gap in the companion mass distribution might be present. The small number of close low-mass companion stars could support the embryo-ejection formation scenario for brown dwarfs. Our findings are compared with and complementary to visual, spectroscopic, and astrometric data on binarity in Sco OB2. We find an overall companion star fraction of 0.52 in this association. This is a lower limit since the data from the observations and from literature are hampered by observational biases and selection effects. This paper is the first step toward our goal to derive the primordial binary population in Sco OB2.

**Key words.** binaries: visual – binaries: general – stars: formation – associations – individual: Sco OB2

### 1. Introduction

Duplicity and multiplicity properties of newly born stars are among the most important clues to understanding the process of star formation (Blaauw, 1991). Observations of star forming regions over the past two decades have revealed two important facts: (1) practically all (70–90%) stars form in clusters (e.g., Lada & Lada, 2003) and, (2) within these clusters most stars are formed in binaries (Mathieu, 1994). Consequently, the star formation community has shifted its attention toward under-

standing the formation of multiple systems — from binaries to star clusters — by means of both observations and theory.

The observational progress in studies of very young embedded as well as exposed star clusters is extensively summarized in the review by Lada & Lada (2003). On the theoretical side the numerical simulations of cluster formation have become increasingly sophisticated, covering the very earliest phases of the development of massive dense cores in giant molecular clouds (e.g., Klessen, Heitsch, & Mac Low, 2000), the subsequent clustered formation of stars and binaries (e.g., Bate, Bonnell, & Bromm, 2003), as well as the early evolution of the binary population during the phase of gas expulsion from

Send offprint requests to: M.B.N. Kouwenhoven e-mail: kouwenho@science.uva.nl

the newly formed cluster (Kroupa, Aarseth, & Hurley, 2001). At the same time numerical simulations of older exposed clusters have become more realistic by incorporating detailed stellar and binary evolution effects in N-body simulations (e.g., Portegies Zwart et al., 2001). This has led to the creation of a number of research networks that aim at synthesizing the modeling and observing efforts into a single framework which covers all the stages from the formation of a star cluster to its eventual dissolution into the Galactic field, an example of which is the MODEST collaboration (Hut et al., 2003; Sills et al., 2003).

Such detailed models require stringent observational constraints in the form of a precise characterization of the stellar content of young clusters. Investigations of the stellar population in young clusters have mostly focused on single stars. However, as pointed out by Larson (2001), single stars only retain their mass from the time of formation whereas binaries retain three additional parameters, their mass ratio, angular momentum and eccentricity. Thus, the properties of the binary population can place much stronger constraints on the physical mechanisms underlying the star and cluster formation process.

Ideally, one would like an accurate description of the ‘primordial’ binary population. This population was defined by Brown (2001) as “the population of binaries as established just after the formation process itself has finished, i.e., after the stars have stopped accreting gas from their surroundings, but before stellar or dynamical evolution have had a chance to alter the distribution of binary parameters”. This definition is not entirely satisfactory as stellar and dynamical evolution will take place already during the gas-accretion phase.

Here we revise this definition to: “*the population of binaries as established just after the gas has been removed from the forming system, i.e., when the stars can no longer accrete gas from their surroundings*”. This refers to the same point in time, but the interpretation of the ‘primordial binary population’ is somewhat different. The term now refers to the point in time beyond which the freshly formed binary population is affected by *stellar/binary evolution and stellar dynamical effects only*. Interactions with a surrounding gaseous medium no longer take place.

From the point of view of theoretical/numerical models of star cluster formation and evolution the primordial binary population takes on the following meaning. It is the final population predicted by simulations of the formation of binaries and star clusters, and it is the initial population for simulations that follow the evolution of star clusters and take into account the details of stellar dynamics and star and binary evolution. The primordial binary population as defined in this paper can be identified with the initial binary population, defined by Kroupa (1995b) as the binary population at the instant in time when the pre-main-sequence eigenevolution has ceased, and when dynamical evolution of the stellar cluster becomes effective. Kroupa (1995a,c) infers the initial binary population by the so-called inverse dynamical population synthesis technique. This method involves the evolution of simulated stellar clusters forward in time for different initial binary populations, where the simulations are repeated until a satisfactory fit with the present day binary population is found.

Our aim is to obtain a detailed observational characterization of the primordial binary population as a function of stellar mass, binary parameters, and (star forming) environment. The most likely sites where this population can be found are very young (i.e., freshly exposed), low density stellar groupings containing a wide spectrum of stellar masses. The youth of such a stellar grouping implies that stellar evolution will have affected the binary parameters of only a handful of the most massive systems. The low stellar densities guarantee that little dynamical evolution has taken place after the gas has been removed from the forming system. These constraints naturally lead to the study of the local ensemble of OB associations. Star clusters are older and have a higher density than OB associations and are therefore less favorable. For example, in the Hyades and Pleiades, the binary population has significantly changed due to dynamical and stellar evolution (Kroupa, 1995c). Note that OB associations may start out as dense clusters (Kroupa, Aarseth, & Hurley, 2001; Kroupa & Boily, 2002). However, they rapidly expel their gas and evolve to low-density systems. This halts any further dynamical evolution of the binary population.

Brown et al. (1999) define OB associations as “young ( $\lesssim 50$  Myr) stellar groupings of low density ( $\lesssim 0.1M_{\odot}\text{pc}^{-3}$ ) — such that they are likely to be unbound — containing a significant population of B stars.” Their projected dimensions range from  $\sim 10$  to  $\sim 100$  pc and their mass spectra cover the mass range from O stars all the way down to brown dwarfs. For reviews on OB associations we refer to Blaauw (1991) and Brown et al. (1999). Thanks to the *Hipparcos* Catalogue (ESA 1997) the stellar content of the nearby OB associations has been established with unprecedented accuracy to a completeness limit of  $V \sim 10.5$  mag, or about  $1 M_{\odot}$  for the stars in the nearest associations (de Zeeuw et al., 1999; Hoogerwerf, 2000). Beyond this limit the population of low-mass pre-main-sequence stars has been intensively studied in, e.g., the Sco OB2 association (Preibisch et al., 2002; Mamajek et al., 2002).

The latter is also the closest and best studied of the OB associations in the solar vicinity and has been the most extensively surveyed for binaries. The association consists of three subgroups: Upper Scorpius (US, near the Ophiuchus star forming region, at a distance of 145 pc), Upper Centaurus Lupus (UCL, 140 pc) and Lower Centaurus Crux (LCC, 118 pc). The ages of the subgroups range from 5 to  $\sim 20$  Myr and their stellar content has been established from OB stars down to brown dwarfs. (for details see de Geus, de Zeeuw, & Lub, 1989; de Zeeuw et al., 1999; de Bruijne, 1999; Hoogerwerf, 2000; Mamajek et al., 2002; Preibisch et al., 2002). Surveys targeting the binary population of Sco OB2 include the radial-velocity study by Levato et al. (1987), the speckle interferometry study by Köhler et al. (2000), and the adaptive optics study by Shatsky & Tokovinin (2002). Because of their brightness many of the B-star members of Sco OB2 have been included in numerous binary star surveys, in which a variety of techniques have been employed. The literature data on the binary population in Sco OB2 is discussed by Brown (2001) and reveals that between 30 and 40 per cent of the *Hipparcos* members of Sco OB2 are known to be binary or multiple systems.

However, these data are incomplete and suffer from severe selection effects, which, if not properly understood, will prevent a meaningful interpretation of the multiplicity data for this association in terms of the primordial binary population. The first problem can be addressed by additional multiplicity surveys of Sco OB2. In this paper we report on our adaptive optics survey of Sco OB2 which was aimed at surveying all the *Hipparcos* members of spectral type A and late B, using the ADONIS instrument on the 3.6m telescope at ESO, La Silla.

We begin by describing in Sect. 2 our observations, the data reduction procedures and how stellar components other than the target stars were detected in our images. These components have to be separated into background stars and candidate physical companions. We describe how this was done in Sect. 3. The properties of the physical companions are described in Sect. 4. In Sect. 5 we discuss which of the physical companions are new by comparing our observations to data in the literature and we provide updated statistics of the binary population in Sco OB2. We summarize this work in Sect. 6 and outline the next steps of this study which are aimed at addressing in detail the problem of selection biases associated with multiplicity surveys and subsequently characterizing the primordial binary population.

## 2. Observations and data reduction

### 2.1. Definition of the sample

A census of the stellar content of the three subgroups of Sco OB2 based on positions, proper motions, and parallaxes was presented by de Zeeuw et al. (1999). Our sample is extracted from their list of *Hipparcos* member stars and consists of A and B stars. In order to avoid saturating the detector during the observations, we were restricted to observing stars fainter than  $V \sim 6$  mag. The sample therefore consists mainly of late-B and A stars which at the mean distance of Sco OB2 (130 pc) corresponds to stars with  $6 \text{ mag} \lesssim V \lesssim 9 \text{ mag}$ , which translates to very similar limits in  $K_S$ . We observed 199 stars from the resulting *Hipparcos* member sample (Table 1). Not all late-B and A member stars could be observed due to time limitations. The distribution of target stars over spectral type is: 83 (157) B, 113 (157) A, 2 (138) F, and 1 (48) G, where the numbers in brackets denote the total number of Sco OB2 *Hipparcos* members of the corresponding spectral type.

### 2.2. Observations

The observations were performed with the ADONIS/SHARPII+ system (Beuzit et al., 1997) on the ESO 3.6 meter telescope at La Silla, Chile. This is an adaptive optics system coupled to an infrared camera with a NICMOS3 detector array. The field of view of the  $256 \times 256$  pixel detector is  $12.76'' \times 12.76''$ . The plate scale is  $0.0495'' \pm 0.0003''$  per pixel, and the orientation of the field is  $-0^\circ.20 \pm 0^\circ.29$  (measured from North to East)<sup>1</sup>. Wavefront sensing was performed directly on the target stars.

<sup>1</sup> The astrometric calibrations are based on observations of the astrometric reference field ( $\theta$  Ori) for ADONIS/SHARPII+/NICMOS3

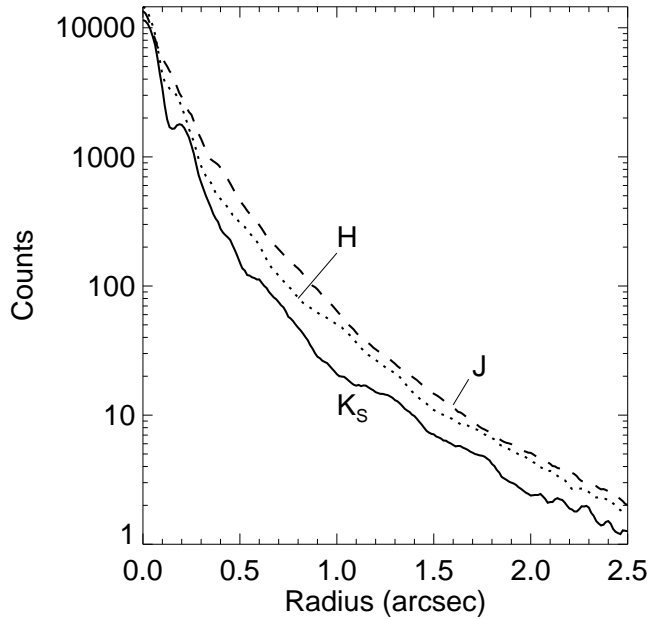


**Fig. 1.** The radial profile of the PSF for the target star HIP53701. The observations are obtained using the ADONIS/SHARPII+ system on June 7, 2001 in  $J$ ,  $H$ , and  $K_S$ . The corresponding Strehl ratios for these observations are 18% in  $J$ , 26% in  $H$  and 31% in  $K_S$ .

Our observing campaign was carried out in two periods: a period from May 31 to June 4, 2000, and one from June 5 to 9, 2001. Out of the eight observing nights about 1.5 were lost due to a combination of bad weather and technical problems. Each target star is observed in the  $K_S$  ( $2.154 \mu\text{m}$ ) band. A subset is additionally observed in the  $J$  ( $1.253 \mu\text{m}$ ) and  $H$  ( $1.643 \mu\text{m}$ ) band. In our search for companion stars, near-infrared observations offer an advantage over observations in the optical. In the near-infrared the luminosity contrast between the primary star and its (often later type) companion(s) is lower, which facilitates the detection of faint companions. The performance of the AO system is measured by the Strehl ratio, which is the ratio between the maximum of the ideal point spread function (PSF) of the system and the measured maximum of the PSF. Typical values for the Strehl ratio in our observations were 5–15% in  $J$ , 15–20% in  $H$  and 20–35% in  $K_S$  (Figure 1).

Each star was observed at four complementary pointings in order to enhance the sensitivity of the search for close companions and to maximize the available field of view (Figure 2). The two components of the known and relatively wide binaries HIP77315/HIP77315 and HIP80324 were observed individually and combined afterwards. For all targets each observation consists of 4 sets of 30 frames (i.e. 4 data cubes). The integration time for each frame was 200 – 2000 ms, depending on the brightness of the source. After each observation, thirty sky frames with integration times equal to those of the corre-

(see <http://www.imcce.fr/priam/adonis>). Mean values for the period 9/1999 to 12/2001 are used. Plate scale and position angle differences between the two observing runs fall within the error bars.

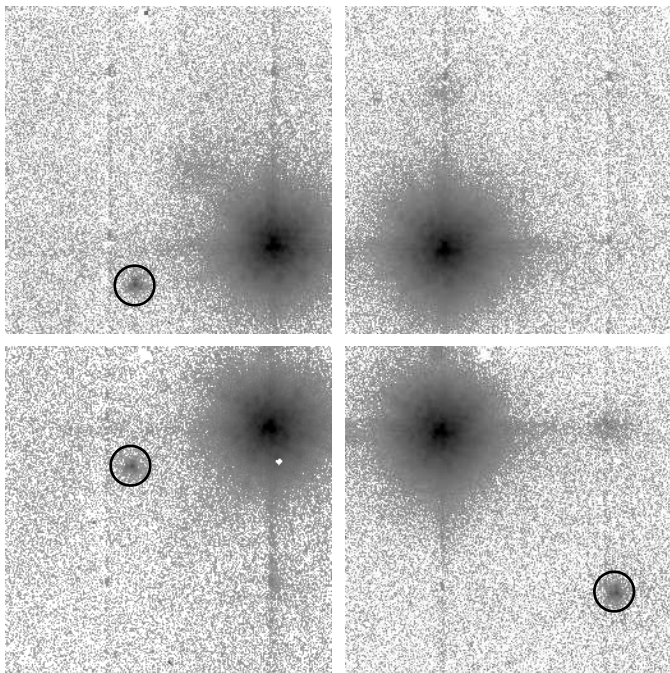


**Fig. 2.** An example illustrating the observing strategy. Observations are obtained with ADONIS/SHARPII+ system in  $J$ ,  $H$ , and  $K_S$ . Four observations of each star are made, each observed with a different offset, in order to maximize the field of view. The frame size of the individual quadrants is  $12.76'' \times 12.76''$ . Combination of the quadrants results in an effective field of view of  $19.1'' \times 19.1''$ . This figure shows  $K_S$  band observations of the A0 V star HIP75957. Two stellar components at angular separations of  $5.6''$  and  $9.2''$  (indicated with the black circles) are detected. These components are visible to the left (East) and bottom-right (South-West) of HIP75957 and are probably background stars. All other features are artifacts.

sponding target star were taken in order to measure background emission. The sky frames were taken 10 arcmin away from the target star and care was taken that no bright star was present in the sky frame. Nevertheless, several sky frames contain faint background stars. The error on the target star flux determination due to these background stars is less than 0.06% of the target star flux and therefore negligible for our purposes. Dark frames and flatfield exposures (using the internal lamp) were taken and standard stars were regularly observed.

We did not use the coronagraph in our setup. The coronagraph obscures most of the target star's flux, which complicates flux calibration of the target stars and their companions. Furthermore, the use of the coronagraph prevents detection of close companions with angular separations less than  $1''$ . The advantage of the coronagraph is that one can detect fainter objects, which would otherwise remain undetected due to saturation of the target stars. However, the large majority of these faint components are likely background stars (see §3).

### 2.3. Data reduction procedures

The primary data reduction was performed with the ECLIPSE package (Devillard, 1997). Information about the sensitivity of each pixel is derived from the (dark current subtracted) flatfield images with different exposure times. The number of counts as a function of integration time is linearly fitted for each pixel. The results are linear gain maps (pixel sensitivity maps) for each filter and observing night. Bad pixel maps for each observing run and filter are derived from the linear gain maps: each pixel with a deviation larger than  $3\sigma$  from the median is flagged as a bad pixel. The average sky map is subtracted from the corresponding standard star and target star data cubes. The resulting data cubes are then corrected using the dark current maps, the linear gain maps, and bad pixel maps.

Image selection and image combination was done with software that was written specifically for this purpose. Before combination, frames with low Strehl ratios with respect to the median were removed. Saturated frames (i.e. where the stellar flux exceeds the SHARPII+ linearity limit) and frames with severe wavefront correction errors were also removed. The other frames were combined by taking the median. Typically, about 2 to 3 out of 30 frames were rejected before combination.

### 2.4. Component detection

We used the STARFINDER package (Diolaiti et al., 2000) to determine the position and instrumental flux of all objects in the images. For each component other than the target star we additionally measured the correlation between the PSF of the target star and that of the component. Components with peak fluxes less than 2 to 3 times the noise in the data, or with correlation coefficients less than  $\sim 0.7$ , were considered as spurious detections.

Since the PSF of the target star is generally not smooth, it was sometimes difficult to decide whether a speckle in the PSF halo of the star is a stellar component, or merely a part of the PSF structure. In this case four diagnostics were used to discriminate between stellar components and PSF artifacts. First, a comparison between the images with the target star located in four different quadrants was made. Objects that do not appear in all quadrants where they *could* be detected were considered artifacts. Second, a similar comparison was done with the individual uncombined raw data frames. Third, a radial profile was fit to the PSF and subtracted from the image to increase the contrast, so that the stellar component becomes more obvious. And finally, a comparison between the PSF of the target star and the PSF of the star previous or next in the program with a similar position on the sky was made by blinking the two images. These two PSFs are expected to be similar and therefore faint close companion stars can be detected.

In total we detect 151 stellar components other than the target stars. A significant fraction of these 151 components are background stars (see §3). All other components are companion stars. Figure 3 shows the  $K_S$  magnitude of the companion and background stars as a function of angular separation  $\rho$  between the target star and the companion or background stars. The same plot also shows  $\Delta K_S = K_{S,\text{component}} - K_{S,\text{primary}}$

as a function of  $\rho$ . Previously unknown companion stars (see § 5.1) and known companions are indicated with the dots and the plusses, respectively. The background stars (see § 3) are represented with triangles. This figure shows that the detection probability of companion stars increases with increasing angular separation and decreasing magnitude difference, as expected. The lower magnitude limit for component detection is determined by the background noise; the lower limit for the angular separation is set by the PSF delivered by the AO system. Note that not all detected components are necessarily companion stars. A simple criterion is used to separate the companion stars ( $K_S < 12$  mag) and the background stars ( $K_S > 12$  mag). See § 3 for the motivation of this choice.

The estimated detection limit as a function of angular separation and companion star flux is represented in Figure 3 with a solid curve. The detection limit is based on  $K_S$  band measurements of simulated companion stars around the B9 V target star HIP65178. In the image we artificially added a second component, by scaling and shifting a copy of the original PSF, thus varying the desired flux and angular separation of the simulated companion. We sampled 30 values for the companion flux linearly in the range  $9.35 \text{ mag} \leq K_S \leq 15.11 \text{ mag}$ , and 40 values for the angular separation between primary and companion linearly in the range  $0.05'' \leq \rho \leq 2''$ . For each value of the angular separation we determined the minimum flux for which the companion star is detectable (i.e. with a peak flux of 2 – 3 times the noise in the data). In order to minimize biases, we repeated this procedure for four different position angles and averaged the results. The standard deviation of the detection limit is  $0.07''$  at a given magnitude and  $0.35 \text{ mag}$  at a given angular separation. Similar simulations with other target stars (e.g., HIP58859, Strehl ratio = 8%; HIP76048, Strehl ratio = 27%) show that the detection limit for the observations with different Strehl ratios is comparable to that of HIP65178 (Strehl ratio = 40%). All target stars are of spectral type A or late-B and have comparable distances. The detection limit shown in Figure 3 is therefore representative for our sample.

## 2.5. Photometry

Near-infrared magnitudes for the observed standard stars are taken from van der Blik, Manfroid, & Bouchet (1996), Carter & Meadows (1995), and the 2MASS catalog. All magnitudes are converted to the 2MASS system using the transformation formulae of Carpenter (2001). The standard stars HD101452, HD190285 and HD96654 were found to be double. The fluxes for the primary and secondary of the standard stars HD101452 and HD96654 are added for calibration, since the secondaries are unresolved in van der Blik, Manfroid, & Bouchet (1996). For HD190285, only the flux of the primary is used for calibration since the secondary is resolved in the 2MASS catalog.

The zeropoint magnitudes are calculated for each observing night and each filter individually. There are non-negligible photometric zeropoint differences between the four detector quadrants. Application of the reduction procedure to simulated observations (but using the ADONIS/SHARPII+ dark frames and

flatfield exposures) also shows this zeropoint offset, unless the flatfielding was omitted. Hence, the zeropoint offset between the four quadrants is caused by large-scale variations in the flatfield exposures. The four detector quadrants were consequently calibrated independently.

Since the distribution of observed standard stars over air-mass is not sufficient to solve for the extinction coefficient  $k$ , we use the mean extinction coefficients for La Silla<sup>2</sup>:  $k_J = 0.081 \text{ mag/airmass}$ ,  $k_H = 0.058 \text{ mag/airmass}$  and  $k_{K_S} = 0.113 \text{ mag/airmass}$ . The standard stars have similar spectral type as the target stars, which allows us to neglect the color term in the photometric solution.

## 3. Background stars

Not all of the 151 stellar components that we find around the target stars are companion stars. The chance that a foreground or background star is present in the field is not negligible. There are several techniques that can be applied to determine whether a detected component is a background star or a probable companion star.

Separation of the objects based on the position of the component in the color-magnitude diagram (CMD) is often applied to discriminate background stars from companion stars (see, e.g., Shatsky & Tokovinin, 2002). Given a certain age of the population, a companion star should be found close to the isochrone that corresponds to that age. When age and distance spread are properly taken into account, this method provides an accurate estimate of the status of the object. We are unable to apply this technique to our data since only a small fraction of our observations is multi-color (see § 4.2 and Figure 10).

Following Shatsky & Tokovinin (2002) we use a simple brightness criterion to separate the companion stars ( $K_S \leq 12$  mag) and the background stars ( $K_S > 12$  mag). At the typical distance of a Sco OB2, an M5 main sequence star has approximately  $K_S = 12$  mag. The three subgroups of Sco OB2 are located at distances of 145, 140, and 118 pc. We assume an age of 5 Myr for US (de Geus, de Zeeuw, & Lub, 1989; Preibisch & Zinnecker, 1999), and 20 Myr for UCL and LCC (Mamajek et al., 2002). Using the isochrones described in § 4.3, we find that stars with  $K_S = 12$  mag correspond to stars with masses of  $0.08 M_\odot$ ,  $0.18 M_\odot$ , and  $0.13 M_\odot$  for US, UCL, and LCC, respectively. Using the  $K_S = 12$  mag criterion we conclude that 77 out of 151 components are likely background stars. The remaining 74 components are thus candidate companion stars.

Although this  $K_S = 12$  mag criterion works well for stars, it is not very accurate below the hydrogen burning limit. Martín et al. (2004) found 28 candidate brown dwarf members of the US subgroup using  $I$ ,  $J$ , and  $K$  photometry from the DENIS database. All members have  $10.9 \text{ mag} \leq K \leq 13.7 \text{ mag}$  and their spectral types are in the range M5.5–M9. According to the  $K_S = 12$  mag criterion, 19 of these brown dwarfs would be classified as companion stars and 8 as background stars (one brown dwarf does not have a  $K$  magnitude entry). A significant

<sup>2</sup> see <http://www.la.s.eso.org/lasilla/sciops/ntt/sofi>

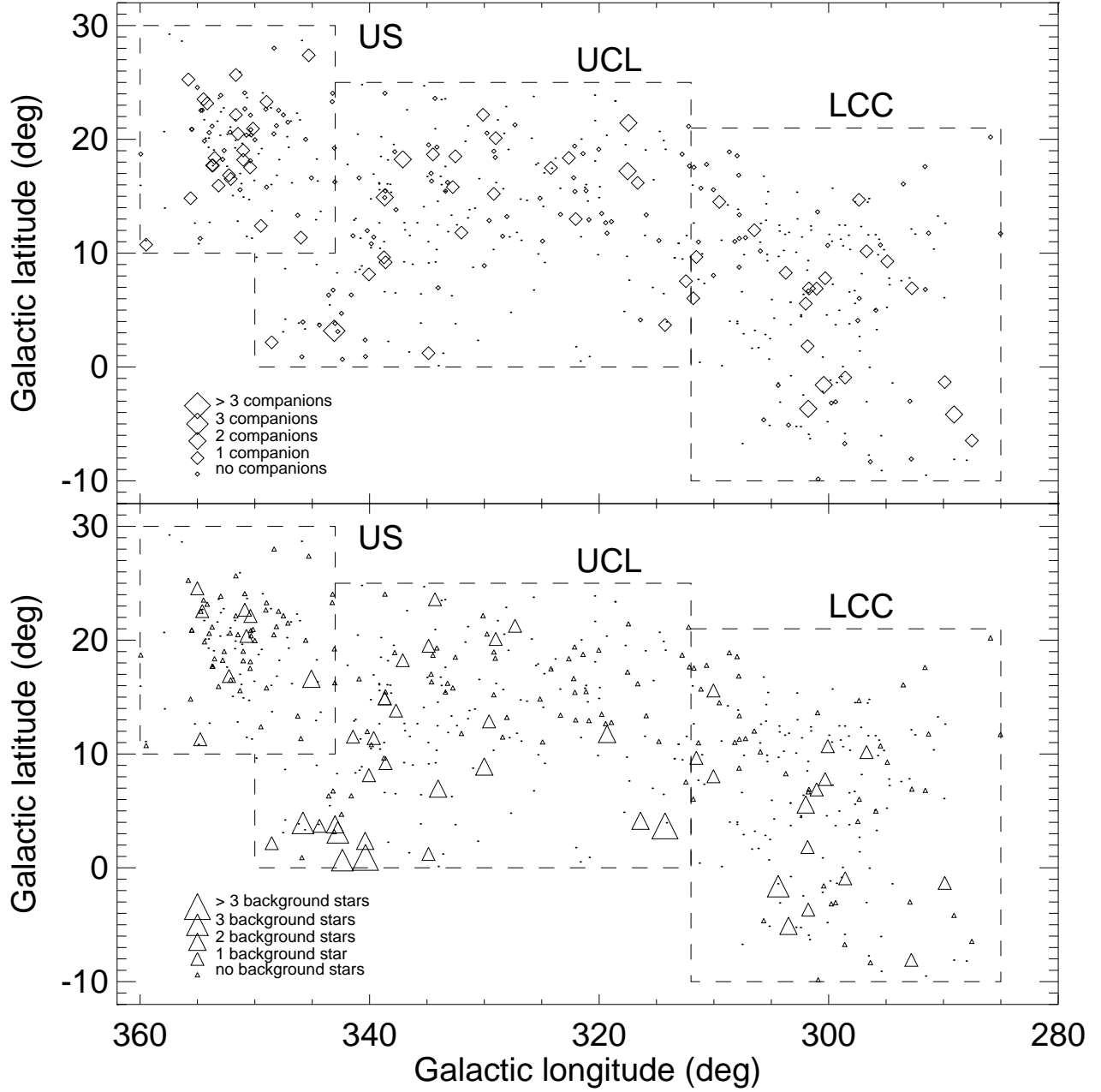


**Fig. 7.** The distribution of 74 detected candidate companions (*top*) and the 77 presumed background stars (*bottom*) over Galactic coordinates. The number of companions and background stars found per target star is indicated by the size of the diamonds and triangles, respectively. *Hipparcos* member stars that were not observed are shown as dots. The borders of the three subgroups of Sco OB2 (Upper Scorpius, Upper Centaurus Lupus, and Lower Centaurus Crux) are indicated by the dashed lines. The background stars are concentrated towards the location of the Galactic plane (see also Figure 8).

fraction of possible brown dwarf companion stars to our observed target stars would be classified as background stars.

In this study we cannot determine with absolute certainty whether a detected component is a companion star or a background star. For example, a foreground star with  $K_S > 12$  mag will not be excluded by the criterion described above. However, the differences between the companion star distribution and the background star distribution can be used to find out if the

results are plausible or not. For this purpose, we derive the expected distribution of background stars per unit of angular separation  $P(\rho)$ , position angle  $Q(\varphi)$ , and  $K_S$  band magnitude  $R(K_S)$  for the background stars.

Background stars are expected to be uniformly distributed over the image field with a surface density of  $\Sigma$  stars per unit

of solid angle. The number of observed background stars  $P(\rho)$  per unit of angular separation  $\rho$  is given by

$$P(\rho) = \frac{d}{d\rho} \int_{\Omega_\rho} \Sigma d\Omega_\rho, \quad (1)$$

where  $\Omega_\rho$  is the part of the field of view contained within a circle with radius  $\rho$  centered on the reference object (the target star). In calculating the expected  $P(\rho)$  for our observations, we assume that the reference object is located in the center of the field of view. For a square field of view with dimension  $L$ , Equation 1 then becomes

$$P(\rho) \propto \begin{cases} 2\pi\rho & \text{for } 0 < \rho < L/2 \\ 8\rho\left(\frac{\pi}{4} - \arccos\frac{L}{2\rho}\right) & \text{for } L/2 < \rho < L/\sqrt{2} \\ 0 & \text{for } \rho > L/\sqrt{2} \end{cases}. \quad (2)$$

For our observing strategy (Figure 2) we have  $L = \frac{3}{2} \cdot 12.76'' = 19.14''$ . For  $\rho \leq L/2 = 9.6''$  the background star density for constant  $K_S$  is proportional to  $\rho$ , after which it decreases down to 0 at  $\rho = L/\sqrt{2} = 13.6''$ . Here we have made the assumption that each target is exactly in the center of each quadrant.

We can also calculate  $Q(\varphi)$ , the expected distribution of background stars over position angle  $\varphi$ . For  $\rho \leq L/2$ ,  $Q(\varphi)$  is expected to be random. For  $L/2 < \rho \leq L/\sqrt{2}$  one expects  $Q(\varphi) = L^2/8 \cos^2 \varphi$  for  $0^\circ \leq \varphi < 45^\circ$ <sup>3</sup>.  $Q(\varphi)$  is undefined for  $\rho > L/\sqrt{2}$ . The above calculations apply to an ideal situation of our observing strategy. In practice, the target star is not always exactly centered in one detector quadrant, which influences  $P(\rho)$  and  $Q(\varphi)$  for  $\rho \gtrsim L/\sqrt{2}$ .

Shatsky & Tokovinin (2002) analysed the background stars in their sky frames taken next to their science targets in Sco OB2. We use their data to derive  $R(K_S)$ , the expected  $K_S$  magnitude distribution for background stars. We fit a second order polynomial to the logarithm of the cumulative  $K_S$  as a function of  $K_S$  of the background stars (Figure 4 in Shatsky & Tokovinin, 2002). In our fit we only include background stars with  $12 \text{ mag} < K_S < 16 \text{ mag}$  since that is the  $K_S$  magnitude range of the presumed background stars. The  $K_S$  magnitude distribution  $f(K_S)$  is then given by the derivative of the cumulative  $K_S$  distribution.

Figure 4 shows the companion star and background star distribution as a function of angular separation. The two distributions are clearly different. The companion stars are more centrally concentrated than the background stars. The solid curve represents  $P(\rho)$ , normalized in such a way that the number of stars corresponds to the expected number of background stars with  $12 \text{ mag} < K_S < 16 \text{ mag}$  (see below and Figure 5). More background stars are present at angular separation  $4'' < \rho < 6''$  relative to what is expected. This is confirmed with a Kolmogorov-Smirnov (KS) test. The KS test is usually quantified with the ‘‘KS significance’’, which ranges from 0 to 1 and corresponds to the probability that the two datasets are drawn from the same underlying distribution. For this KS comparison we only consider those background stars

<sup>3</sup> This formula is also valid for  $90^\circ \leq \varphi < 135^\circ$ ,  $180^\circ \leq \varphi < 125^\circ$ , and  $270^\circ \leq \varphi < 315^\circ$ .  $Q(\varphi) = L^2/8 \sin^2 \varphi$  for all other position angles between  $0^\circ$  and  $360^\circ$ .

with  $\rho \leq L/\sqrt{2} = 9.6''$ . For background stars with  $\rho > 9.6''$  we expect the predicted distribution to differ slightly from the observed distribution (see above). We find a KS significance level of  $1.8 \times 10^{-4}$ , which implies that the excess of background stars with  $4'' < \rho < 6''$  is real, assuming that the simple model for the angular separation distribution is correct. The excess of close background stars might be caused by faint ( $K_S > 12 \text{ mag}$ ) companion stars which are misclassified as background stars.

The position angle distribution of companion stars and background stars is shown in Figure 6. The objects are expected to be randomly distributed over position angle for  $\rho \leq L/2 = 9.6''$ , which is illustrated in Figure 6. For objects with  $\rho \leq L/2 = 9.6''$  we find that, as expected, the position angle distribution is random, for both the companion stars (KS significance level 0.86) and the background stars (KS significance level 0.84). For angular separations larger than  $9.6''$  the objects are primarily found in the ‘corners’ of the image ( $\varphi = 45^\circ, 135^\circ, 225^\circ, 315^\circ$ ).

The expected number of background stars per unit of angular separation and unit of magnitude,  $R(K_S)P(\rho)$  is plotted in Figure 5. We observe 19 background stars in the region  $14 \text{ mag} \leq K_S \leq 15 \text{ mag}$  and  $5'' \leq \rho \leq 13''$  and normalize the theoretical background star density accordingly. The brightness of the PSF halo can explain the smaller number of background stars than expected for  $\rho \lesssim 2.5''$  and  $K_S \gtrsim 15 \text{ mag}$ . The predicted strong decline in background stars for  $\rho \gtrsim 10''$  is present in the observations. Few background objects with  $12 \text{ mag} < K_S < 14 \text{ mag}$  are expected in the angular separation range of  $2'' - 4''$ .

The distribution of the detected candidate companions and background stars on the sky is shown in Figure 7. The covered fields close to the Galactic plane include a larger number of background stars, as expected. This is even better visible in Figure 8, which shows the distribution of observed objects over Galactic latitude. The distribution of Sco OB2 *Hipparcos* member stars over Galactic latitude is similar to that of the companion stars.

In principle, it is also possible that another (undocumented) member star of Sco OB2 projects close to the target star. The status of these stars (companion star or ‘‘background star’’) cannot be determined with the CMD or the  $K_S = 12 \text{ mag}$  criterion. Preibisch et al. (2002) estimate the number of member stars in the US subgroup in the range  $0.1 - 20 M_\odot$  to be about 2500. This corresponds roughly to a stellar surface density of  $8 \times 10^{-7}$  star arcsec<sup>-2</sup>. The chance of finding another US member star (i.e. not a binary companion) in a randomly pointed observation of US is of the order 0.03%. The detection probabilities for the other two subgroups of Sco OB2 are similarly small and negligible for our purpose.

## 4. Properties of the companion stars

### 4.1. General properties

The angular separation distribution of the companion stars is centrally concentrated (Figures 4 and 6). The error in the angular separation is typically  $0.0015''$ . Faint ( $K_S \gtrsim 11 \text{ mag}$ ) objects with angular separation less than  $\rho \approx 0.8''$  cannot be

detected in the presence of the PSF halo of the bright primary star, while the upper limit of  $13.5''$  is determined by the field of view. The distribution over position angle is random for  $\rho \leq L/2 = 9.6''$ , as expected (see § 3). The median error in position angle is  $0.03^\circ$ , increasing with decreasing angular separation.

Two observed systems are clearly hierarchical triples where a double 'secondary' orbits the primary star. These are HIP68532, where the double 'secondary' has  $\rho = 3.1''$  and  $\varphi = 290^\circ$ , and HIP69113, with  $\varphi = 65^\circ$  and  $\rho = 5.4''$ . HIP69113 has a third companion star with  $\rho = 28.6''$  and  $\varphi = 35^\circ$  Dufloot, Figon, & Meyssonier (1995). This star is not observed in our survey because of the large distance from the primary star. The nature of the HIP69113 system is extensively discussed by Huéramo et al. (2001). Figure 9 shows HIP68532 and HIP69113 with companion stars. The target stars HIP52357, HIP61796, and HIP81972 also have two companion stars. The two companion stars of each of these systems have approximately the same angular separation and position angle, but it is unclear whether these systems are hierarchical in the way described above.

The 199 observed primaries have a  $K_S$  magnitude range of 5.2 – 8.3 mag. The  $K_S$  magnitudes of the companion stars (Figure 3) range from  $K_S = 6.4$  mag to 12.0 mag, the upper limit resulting from the criterion that was used to remove the background stars from the sample. The primaries in our sample all have similar spectral type, distance, and interstellar extinction. The magnitude of the companions relative to that of their primaries,  $\Delta K_S$ , spans the range from 0.0 mag to 6.0 mag. The median error is 0.05 mag in  $J$ , 0.04 mag in  $H$ , 0.07 mag in  $K_S$ , and 0.075 mag in  $J - K$ .

Properties of the 199 target stars, 74 candidate companion stars, and 77 presumed background stars are listed in Table 1. The name of the star is followed by the  $J$ ,  $H$ , and  $K_S$  magnitude. If the magnitude is derived from measurements done under non-photometric conditions, a remark is placed in the last column. The spectral type of each primary is taken from the *Hipparcos* catalogue. The angular separation and position angle (measured from North to East) are derived from the combination of all available observations for a particular star. For each star we also list the status (p = primary star, c = candidate companion star, nc = new candidate companion star, b = background star) and the subgroup membership.

#### 4.2. Color-magnitude diagram and isochrones

In § 3 we mentioned that it is possible to separate background stars and companion stars using their position in the CMD. In this section we derive the absolute magnitude  $M_{K_S}$  for all observed objects. We additionally derive colors for objects with multi-color observations. Only measurements obtained under photometric conditions are used. We construct a CMD and determine whether the observed components are background stars or companion stars by comparing their position in the CMD to that of the isochrones. In § 4.3 we will use the absolute magnitude  $M_{K_S}$  and the isochrones to derive the masses of the primary and companion stars.

We calculate the absolute magnitude  $M_{K_S}$  using the distance  $D$  and extinction  $A_{K_S}$  for each target star individually. In de Bruijne (1999) the distance to the Sco OB2 member stars is derived from the secular parallax  $\pi_{\text{sec}}$ . The secular parallax is calculated from the observed positions and proper motions of member stars, where the fact that all stars in an association share the same space motion is exploited. The secular parallax can be up to more than two times as precise compared to the *Hipparcos* parallax. Secular parallaxes with  $g = 9$  are used when available, and with  $g = \infty$  otherwise ( $g$  measures the model-observation discrepancy; see de Bruijne, 1999, for details). The interstellar extinction is also taken from de Bruijne (1999). For the stars that do not have an extinction entry in de Bruijne (1999), an estimate of the extinction is calculated using:

$$A_{K_S} = R_V \times E(B - V)/9.3, \quad (3)$$

where  $R_V = 3.2$  is the standard ratio of total-to-selective extinction (see, e.g., Savage & Mathis, 1979). The value 9.3 is the ratio between  $V$  band and  $K_S$  band extinction (Mathis, 1990), and  $E(B - V) = (B - V) - (B - V)_0$  is the color excess.  $(B - V)$  is the color listed in de Bruijne (1999). The theoretical color  $(B - V)_0$  is derived from the spectral type using the broadband data for main sequence stars in Kenyon & Hartmann (1995). The extinction for the UCL member HIP68958 (spectral type Ap...) is not listed in de Bruijne (1999) and could not be derived from Kenyon & Hartmann (1995). We therefore take  $A_{V,\text{HIP68958}} = 0.063$  mag. This is the median  $A_V$  value for those UCL member stars which have full photometric data in de Bruijne (1999).

Only for a subset of observed targets observations in more than one filter are available; the corresponding CMDs are plotted in Figure 10. The observed primary stars are all of similar spectral type but show scatter in  $M_{K_S}$ ,  $J - K$ , and  $H - K$ . This can be explained by the errors in near-infrared photometry, which are typically 0.07 mag for our observations. The uncertainties in the parallax and reddening introduce an additional error when calculating the absolute magnitudes. Median errors in  $M_J$  and  $M_K$  are consequently about 0.36 mag. The colors  $J - K$  and  $H - K$  have median errors of 0.02 mag and 0.06 mag, respectively.

Given the age of the three Sco OB2 subgroups, not all objects are expected to be positioned on the main sequence. For the young age of Sco OB2, stars of spectral type G or later have not reached the main sequence yet, while the O stars have already evolved away from the main sequence. The age differences between the Sco OB2 subgroups are relatively well-determined. Different values for the absolute ages are derived from the kinematics of the subgroups (Blaauw, 1964, 1978) and stellar evolution (de Zeeuw & Brand, 1985; de Geus, de Zeeuw, & Lub, 1989; Preibisch et al., 2002; Mamajek et al., 2002; Sartori, Lépine, & Dias, 2003). The age of the US subgroup is 5 Myr, without a significant age spread (de Zeeuw & Brand, 1985; de Geus, de Zeeuw, & Lub, 1989; Preibisch et al., 2002). Mamajek et al. (2002) derive an age between 15 and 22 Myr for members of UCL and 17 and 23 Myr for members of LCC. In this paper we adopt an age of 20 Myr for both UCL and LCC.

Star	<i>J</i> mag	<i>H</i> mag	<i>K<sub>S</sub></i> mag	spectral type	$\rho$ (")	<i>PA</i> (°)	status	subgroup	remarks
HIP50520			6.23	A1V			p	LCC	
			6.39		2.51	313.3	c		
HIP52357			7.64	A3IV			p	LCC	
			7.65		0.53	73.0	c		
			11.45		10.04	72.7	nc		
HIP53524			6.76	A8III			p	LCC	
			12.67		4.87	316.9	b		
HIP53701	6.30	6.37	6.48	B8IV			p	LCC	
	9.05	8.76	8.86		3.88	75.8	c		
	13.06	12.93	13.04		6.57	120.1	b		
HIP54231			6.75	A0V			p	LCC	
HIP55188			7.43	A2V			p	LCC	
HIP55899			7.07	A0V			p	LCC	
HIP56354			5.78	A9V			p	LCC	
...	...	...	...	...	...	...	...	...	...

**Table 1.** Results from the ADONIS adaptive optics survey among 199 Sco OB2 member stars. The columns list: *Hipparcos* number, observed *J*, *H* and *K<sub>S</sub>* magnitude, spectral type of the primary, angular separation (arcsec), position angle (degrees; measured from North to East), and status (p = primary; c = companion star; nc = new companion star; b = background star). The last two columns list the subgroup of which the system is a member (US = Upper Scorpius; UCL = Upper Centaurus Lupus; LCC = Lower Centaurus Crux), and a flag in case the observing conditions were not photometric. The *Hipparcos* member stars HIP77315 and HIP77317 are a common proper motion pair (see the Double Star Catalog). In this paper the two stars are treated as separate primaries and not as one system. Table 1 is presented in its entirety in the electronic edition of *Astronomy & Astrophysics*. A portion is shown here for guidance regarding its form and content.

We construct isochrones which are very similar to those described in Preibisch et al. (2002). For the low-mass stars ( $M < 0.7 M_{\odot}$ ) we use exactly the same isochrone as Preibisch et al. (2002): we use the models from Chabrier et al. (2000), which are based on those from Baraffe et al. (1998). For  $0.02 \leq M/M_{\odot} < 0.7$  we take the models with  $[M/H] = 0$  and  $L_{\text{mix}} = H_p$ , where  $L_{\text{mix}}$  is the mixing length and  $H_p$  the pressure scale height. For  $0.7 \leq M/M_{\odot} < 1$  we use the models with  $[M/H] = 0$  and  $L_{\text{mix}} = 1.9H_p$ . We use the models described in Palla & Stahler (1999) for  $1 \leq M/M_{\odot} < 2$ . Near-infrared magnitude tracks, derived using the procedure described in Testi, Palla, & Natta (1998), were kindly provided by F. Palla. Finally, for  $M/M_{\odot} > 2$  we use the models from Girardi et al. (2002) (based on Bertelli et al., 1994) with  $Y = 0.352$  and  $Z = 0.05$ , where  $Y$  and  $Z$  are the helium and metal abundance, respectively.

The resulting 5 Myr isochrone (for US) and 20 Myr isochrone (for UCL and LCC) are plotted in Figure 10. Both isochrones are continuous. Figure 11 shows the relationship between stellar mass and *K*-band absolute magnitude for 5 Myr and 20 Myr populations. The gray-shaded area in Figures 10 and 11 is enclosed by the 15 Myr and 23 Myr isochrones, and shows the effect of the age uncertainty in the UCL and LCC subgroups.

The positions of the primary and companion stars in the CMD are consistent with the isochrones (except the companion of the LCC member star HIP53701). No obvious correlation of the position of these primaries in the CMD with spectral type is present due to the errors in the colors and magnitudes. The presumed background stars are located far from the isochrones in the CMD, supporting our hypothesis that they are indeed background stars.

In Figure 10 we added the candidate brown dwarf members in US from Martín et al. (2004). We estimate the absolute magnitude of these brown dwarfs using the mean US distance of 145 pc and the mean extinction  $A_K = 0.050$  mag (see below). The colors and magnitudes of these objects are consistent with the 5 Myr isochrone (solid curve), as is expected for US member stars.

### 4.3. Masses and mass ratios

We derive the mass of the primary and companion stars from their  $M_{K_S}$  magnitude using the isochrones described in § 4.2 (Figures 10 and 11). We use the 5 Myr isochrone for US and the 20 Myr isochrone for UCL and LCC. The conversion from  $M_{K_S}$  to mass is most accurate for B- and A-type stars, where the absolute value of the derivative  $dM/dM_{K_S}$  is small. We find masses between  $1.4 M_{\odot}$  and  $7.7 M_{\odot}$  for the primaries and masses between  $0.1 M_{\odot}$  and  $3.0 M_{\odot}$  for the companions. Given the error  $\Delta M_{K_S}$  on  $M_{K_S}$ , we calculate for each star the masses  $M_-$  and  $M_+$  that correspond to  $M_{K_S} - \Delta M_{K_S}$  and  $M_{K_S} + \Delta M_{K_S}$ . We define the error on the mass to be  $\frac{1}{2}(M_+ - M_-)$ . The median of the error in the mass, which is a lower limit for the real error, is  $0.4 M_{\odot}$  for the primaries and  $0.1 M_{\odot}$  for the companions.

Figure 12 (top) shows the mass distribution of the companion stars and of the primary stars to which they belong. The mass distribution of the observed target stars without companions is similar to the latter. The plot showing companion star mass as a function of angular separation (Figure 12, bottom) closely resembles Figure 3. The reason for this is that the companion star mass is derived from the  $K_S$  magnitude.

The mass ratio  $q$  and error are calculated for each primary-companion pair. The median formal error on the mass ratio

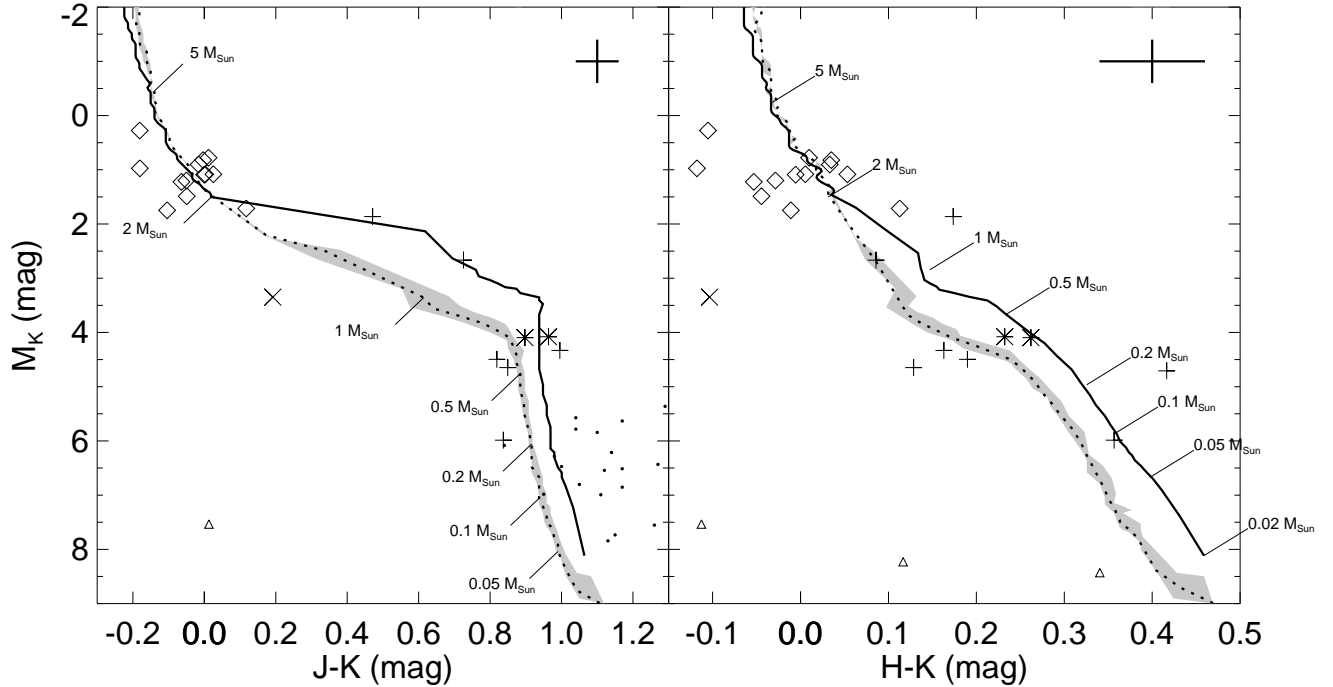


**Fig. 10.** The color-magnitude diagram of the primaries, companion stars and background stars for which we obtained ADONIS/SHARPII+ multi-color AO observations. The  $M_{K_s}$  magnitudes are corrected for distance and extinction. Companion stars in the three different subgroups are indicated with pluses (US), asterisks (UCL) and crosses (LCC). Target stars and background stars are indicated with diamonds and triangles, respectively (see § 3). The curves represent isochrones of 5 Myr (solid curve) and 20 Myr (dotted curve). The 15 Myr and 23 Myr isochrones enclose the gray-shaded area and represent the uncertainty in the age of the UCL and LCC subgroups. The mass scale is indicated for the 20 Myr isochrone (*left*) and the 5 Myr isochrone (*right*). The brown dwarf candidates identified by Martín et al. (2004) are indicated as dots. The median formal errors are indicated as error bars in the top-right corner of each plot. The locations of the target stars and companion stars are consistent with the isochrones (within the error bars). The presumed background stars are located far away from the isochrones, implying that our criterion to separate companion stars and background stars is accurate.

is 0.07 and is to first order proportional to that of the companion star mass. The real error on the mass ratio is most likely larger than the formal error stated above. As indicated by Shatsky & Tokovinin (2002), the mass ratio of a system primarily depends on the magnitude difference between primary and secondary.

The mass ratio distribution is shown in Figures 13 and 14. The smallest mass ratios are found for the companions of HIP80474 ( $q = 0.022 \pm 0.008$ ) and HIP77911 ( $q = 0.035 \pm 0.012$ ). This corresponds well with the expected minimum value for  $q$ : a typical primary in our sample has spectral type A0 V ( $2 M_{\odot}$ ), while the least massive companions considered have  $K_s = 12$  mag ( $\sim 0.1 M_{\odot}$ ), giving  $q = 0.05$ . The systems with large mass ratio ( $q > 0.9$ ) are HIP80324 ( $q = 0.91 \pm 0.23$ ), HIP50520 ( $q = 0.93 \pm 0.19$ ), HIP80238 ( $q = 0.94 \pm 0.29$ ), HIP64515 ( $q = 0.94 \pm 0.15$ ), HIP61639 ( $q = 0.95 \pm 0.15$ ), and HIP52357 ( $q = 1.00 \pm 0.34$ ). Note that for these systems the possibility that  $q > 1$  is included. Due to the error in the mass it is not possible to say which star in these systems is more massive, and hence, which is the primary star. Although the uncertainty in the age of UCL and LCC is not negligible, the

effect on the mass ratio distribution is small (gray-shaded areas in Figure 14).

Following Shatsky & Tokovinin (2002) we fit a power-law of the form  $f(q) = q^{-\Gamma}$  to the mass ratio distribution. We find that models with  $\Gamma = 0.33$  fit our observations best (KS significance level 0.33). The error in  $\Gamma$  due to the age uncertainties in the UCL and LCC subgroups is 0.02. This is in good agreement with Shatsky & Tokovinin (2002), who surveyed 115 B-type stars in Sco OB2 for binarity and observed 37 physical companions around these stars. They find  $\Gamma = 0.3 - 0.5$  for their mass ratio distribution. We observe an excess of systems with  $q \sim 0.1$  with respect to what is expected for models with  $\Gamma = 0.33$ . This could partially be explained by bright background stars that are misclassified as companion stars, but this is unlikely to be an important effect (see § 3). The observational biases (e.g. the detection limit) are not taken into account here. For a more detailed description of the effect of observational biases on the mass ratio distribution we refer to Hogeveen (1990) and Tout (1991).

The cumulative mass ratio distribution  $F(q)$  can also be described as a curve consisting of two line segments. We fit and find that the mass ratio distribution closely follows the function

$$F(q) = \begin{cases} 2.63q - 0.067 & \text{for } 0.03 < q \leq 0.19 \\ 0.72q + 0.294 & \text{for } 0.19 < q \leq 0.97, \end{cases} \quad (4)$$

with a root-mean-square residual of 0.019 (see Figure 14).

We investigate whether the observed mass ratio distribution could be the result of random pairing between primary stars and companion stars, such as observed for solar-type stars in the solar neighbourhood (Duquennoy & Mayor, 1991). To this end, we use Monte Carlo simulations to calculate the mass ratio distribution that is expected for random pairing.

The current knowledge about the brown dwarf population in Sco OB2 is incomplete (e.g., Table 2 in Preibisch, Stanke, & Zinnecker, 2003). Therefore we make a comparison with the mass ratio distribution resulting from two different initial mass functions (IMFs) ( $\text{IMF}_{-0.3}$  and  $\text{IMF}_{2.5}$ ), which differ in slope  $dN/dM$  for substellar masses.

$$\text{IMF}_\alpha : \frac{dN}{dM} \propto \begin{cases} M^\alpha & \text{for } 0.02 \leq M/M_\odot < 0.08 \\ M^{-0.9} & \text{for } 0.08 \leq M/M_\odot < 0.6 \\ M^{-2.8} & \text{for } 0.6 \leq M/M_\odot < 2 \\ M^{-2.6} & \text{for } 2 \leq M/M_\odot < 20, \end{cases} \quad (5)$$

For  $M \geq 0.10 M_\odot$   $\text{IMF}_\alpha$  is equal to the IMF in US that was derived by Preibisch et al. (2002). The Preibisch et al. (2002) IMF is extrapolated down to  $M = 0.08 M_\odot$ . For  $0.02 \leq M/M_\odot < 0.08$  we consider  $\alpha = -0.3$  (Kroupa, 2002) and  $\alpha = 2.5$  (Preibisch, Stanke, & Zinnecker, 2003, Fit I). Most other models described in Preibisch, Stanke, & Zinnecker (2003) have  $-0.3 < \alpha < 2.5$  for  $0.02 \leq M/M_\odot < 0.08$ .

We draw the primary and secondary stars from  $\text{IMF}_\alpha$ . Primary and secondary masses are independently drawn from the mass range  $[0.02, 20] M_\odot$  and are swapped if necessary, so that the primary star is the most massive. Only those systems with primary mass larger than  $1.4 M_\odot$  and smaller than  $7.7 M_\odot$  are considered. We calculate the resulting mass ratio distribution. A KS comparison between the mass ratio distribution resulting from random pairing and the observed distribution shows that the random-pairing hypothesis can be rejected for both  $\text{IMF}_{-0.3}$  and  $\text{IMF}_{2.5}$ . This is clearly visible in Figure 14.

Random pairing requires more systems with low mass ratio than we observe. The error in the mass ratio (ranging between 0.008 and 0.34) cannot compensate for the lack of faint companions. Even if all close ( $\rho \leq 4$ ) background stars are treated as low-mass companions, random pairing is excluded. Hence, there is a deficit of low-mass companions around late-B and A type stars compared to what is expected from random pairing.

Several observed primary stars are actually unresolved binary systems. Since we derive the mass for this 'primary' using the total  $K_S$  flux of such an unresolved system, we introduce an error in the mass and hence the mass ratio. Out of the 199 observed primary stars 18 are known spectroscopic binaries (14 in US, 3 in UCL, and 1 in LCC). These binary systems are too tight to be resolved in our AO survey. We observe companion stars around three of these primaries: HIP77911, HIP77939, and HIP79739 (all in US). For these systems we expect the

mass ratio, which we define here as the mass of the companion star divided by the total mass of the inner part of the system, to deviate significantly from the value derived from our near-infrared observations.

A closer inspection of Figure 3 reveals a lack of stellar components with  $\rho \leq 3.75''$  and  $12 \text{ mag} \lesssim K_S \lesssim 14 \text{ mag}$ . If companion stars or background stars with these properties exist, we should have seen them. In § 3 we showed that few background stars are expected in this region. For example, the brown dwarfs (M5.5–M9) detected by Martín et al. (2004) in US have  $11 \text{ mag} \lesssim K \lesssim 14 \text{ mag}$ . If similar objects within  $\rho \leq 3.75''$  were present, they would have been detected. This 'gap' is not the result of observational biases: the detection limit shows that objects with these properties are detectable.

In order to find out if this 'gap' is expected, we generate a stellar population using a Monte Carlo process and two-dimensional two-sample KS tests. For comparison with the simulated data we only consider the 59 observed companion and background stars with  $\rho \leq 4''$ . Objects with  $\rho > 4''$  are not relevant for this test and might introduce biases due to observational selection effects. We randomly draw primary and secondary masses in the mass range  $[0.02, 20] M_\odot$ . We select only those binaries for which the primary mass is in the range  $[1.4, 7.7] M_\odot$ . Sets of 59 binary systems are created for  $\text{IMF}_{-0.3}$  and  $\text{IMF}_{2.5}$  (Equation 5). The masses are converted into  $K_S$  magnitudes using a distance of 145 pc and the 5 Myr isochrone described in § 4.2. The angular separations for the secondaries are drawn from a uniform distribution in  $[0'', 4'']$ . We create  $10^3$  realizations which are compared to the observations. For  $\text{IMF}_{-0.3}$  we find a mean KS significance level of  $3.5 \times 10^{-3}$ , while for  $\text{IMF}_{2.5}$  we find  $3.2 \times 10^{-3}$ . We repeated the procedure described above with another angular separation distribution:  $\partial N/\partial \rho \propto \rho$  for  $\rho \in [0'', 4'']$  (Öpik's law). We find mean KS significance levels of  $8.2 \times 10^{-5}$  and  $6.5 \times 10^{-5}$  for  $\text{IMF}_{-0.3}$  and  $\text{IMF}_{2.5}$ , respectively. It is therefore unlikely that the observed distribution (including the 'gap') is drawn from the IMFs and angular separation distributions as described above.

Several faint close components with  $\rho \leq 3.75''$  below the 'gap' ( $K_S \gtrsim 14 \text{ mag}$ ) are detected. These objects are found next to the target stars HIP61265, HIP67260, HIP73937, HIP78968, HIP79098, HIP79410, and HIP81949. The Strehl ratios in  $K_S$  of the corresponding observations ( $\sim 20\%$ ) are typical. The detection of these close, faint components therefore cannot be explained by a better performance of the AO system during the observation of these objects. The target stars corresponding to these objects are not particularly faint; the luminosity contrast between the target star and the faint close components is typical. These objects are background stars according to our selection criterion. However, there is a possibility that these objects are close brown dwarfs with masses  $\lesssim 0.05 M_\odot$ , where the conversion from  $K_S$  to mass is strongly dependent on the age. This result implies that A and late-B stars do not have close companions with a mass less than about  $0.1 M_\odot$ , unless the assumed background stars are physical companions (and thus brown dwarfs). If so, a gap would be present in the companion mass distribution.

Reference	Detection method
Alencar et al. (2003)	Spectroscopic
Balega et al. (1994)	Visual
Barbier-Brossat, Petit, & Figon (1994)	Spectroscopic
Batten, Fletcher, & MacCarthy (1997)	Spectroscopic
Couteau (1995)	Combination
The Double Star Library	Combination
Duflot, Figon, & Meyssonier (1995)	Spectroscopic
Hartkopf, McAlister, & Mason (2001)	Visual
Jordi et al. (1997)	Eclipsing
The <i>Hipparcos</i> and <i>Tycho</i> Catalogues	Astrometric
Kraicheva et al. (1989)	Spectroscopic
Malkov (1993)	Combination
Mason (1995)	Visual
McAlister et al. (1993)	Visual
Miscellaneous, e.g. SIMBAD	Combination
Miura et al. (1992)	Visual
Pedoussaut et al. (1996)	Spectroscopic
Shatsky & Tokovinin (2002)	Visual
Sowell & Wilson (1993)	Visual
Svechnikov & Bessonova (1984)	Combination
Tokovinin (1997)	Combination
Worley & Douglass (1997)	Combination

**Table 2.** References to literature data with spectroscopic, astrometric, eclipsing, and visual binaries in Sco OB2. Using these data we find that 33 out of the 74 candidate companion stars in our dataset were already documented in literature, while 41 were previously unknown.

## 5. Comparison with literature data

### 5.1. New companions

We compiled a list of known companion stars to all *Hipparcos* members of Sco OB2 using literature data on binarity and multiplicity. This includes spectroscopic, astrometric, eclipsing, and visual binaries. The references used are listed in Table 2.

Since the angular separation and position angle of companion stars change as a function of time, one has to take care that a ‘newly’ detected companion is not a displaced known companion star. It is therefore interesting to estimate how fast the angular separation and position angle change for the observed companion star. We obtained the primary mass  $M_p$  and companion star mass  $M_s$  in (§ 4.3) thus we can estimate the orbital period of the companion stars using Kepler’s third law. If the orbit is circular and the system is seen face-on, the orbital period is given by  $P = \sqrt{4\pi^2(D\rho)^3/G(M_p + M_s)}$ , where  $D$  is the distance to the system,  $\rho$  the angular separation between primary and companion star, and  $G$  is the gravitational constant. In general, orbits are eccentric and inclined. However, the effect of nonzero eccentricity and inclination on the period is most likely only of the order of a few per cent (Leinert et al., 1993).

In our survey we are sensitive to orbits with a period between approximately 50 yr and 50,000 yr. For most of the systems in our sample we find an orbital period of the order of a few thousand years. The literature data that we used are several decades old at most. The angular separation and position angle are not expected to have changed significantly over this time. If a star with significantly different values for  $\rho$  and/or  $\varphi$

Type	B1-B3	B4-B9	A	F	GKM
<b>Upper Scorpius</b>					
Single stars	3	13	20	17	10
Visual	15	9	12	3	2
Astrometric	0	3	1	2	3
Spectroscopic	11	12	0	0	0
<b>Upper Centaurus Lupus</b>					
Single stars	3	22	41	43	22
Visual	15	23	29	7	8
Astrometric	2	1	3	5	2
Spectroscopic	11	6	1	1	0
<b>Lower Centaurus Crux</b>					
Single stars	3	16	31	47	14
Visual	7	13	24	10	4
Astrometric	1	3	3	4	4
Spectroscopic	3	3	1	0	0
<b>Scorpius OB2</b>					
Single stars	9	51	92	107	46
Visual	37	45	65	20	14
Astrometric	3	7	7	11	9
Spectroscopic	25	21	2	1	0

**Table 3.** Binarity data for Sco OB2, showing the number of companion stars found with the different techniques. Literature data and the new companion stars described in this paper are included. The terms ‘visual’, ‘astrometric’, and ‘spectroscopic’ pertain only to available observations and not to intrinsic properties of the systems. Note that each companion of a multiple system is included individually.

is discovered with respect to the known companion star, this star is considered to be new. Several close binary systems are observed. The shortest orbital periods that we find (assuming circular and face-on orbits) are those for the companions of HIP62026 (57 yr), HIP62179 (68 yr), HIP76001 (84 yr), HIP64515 (87 yr), HIP80461 (106 yr), HIP62002 (142 yr), and HIP67260 (213 yr). Differences in angular separation  $\rho$  and position angle  $\varphi$  are therefore expected with respect to previous measurements. For example, the observed star HIP76001 has two companions with angular separations  $\rho_1$  and  $\rho_2$ , and position angles  $\varphi_1$  and  $\varphi_2$ , respectively. In our AO survey we measure  $(\rho_1, \varphi_1) = (0.25'', 3.2^\circ)$  and  $(\rho_2, \varphi_2) = (1.48'', 124.8^\circ)$ , while Tokovinin (1997) quotes  $(\rho_1, \varphi_1) = (0.094'', 6^\circ)$  in 1993 and  $(\rho_2, \varphi_2) = (1.54'', 130^\circ)$  in 1991. Taking the changes in  $\rho$  and  $\varphi$  into account, we determine whether an observed companion star was documented before or whether it is new.

Table 3 summarizes the current status on binarity for Sco OB2. The number of presently known companion stars is listed as a function of primary spectral type and detection method.

We define all companions that have only been detected with radial velocity studies as spectroscopic. All companions of which the presence of the companion has only been derived from astrometric studies of the primary are classified as astrometric. All other companions, i.e. those that have been detected with (AO) imaging, Speckle techniques, interferometry, etc., are classified as visual. Note that our classification refers only

to available observations and *not* to intrinsic properties of the binary or multiple systems.

All candidate companions that are found with our AO survey are by definition visual. The overlap between the observed companions in our sample and the spectroscopic and astrometric binaries in literature is zero, although HIP78809 is flagged as “suspected non-single” in the *Hipparcos* catalogue. From our comparison with literature we find 41 new companions (14 in US; 13 in UCL; 14 in LCC), while 33 of the candidate companion stars were already documented.

Several of the stars currently known as ‘single’ could be unresolved systems. For a subset of the member stars, multiple companions have been detected using different techniques. Most systems with early spectral type primaries are found with spectroscopic methods. Amongst the A and F type stars, most *Hipparcos* member stars are single, although a fraction of these could be unresolved systems (see § 5.2).

Of the Sco OB2 *Hipparcos* member stars 37 are now known to be triple. Sixteen of these consist of a primary with two visual companions. Fifteen consist of a primary, a visual companion, and a spectroscopic companion. These are only found in UCL and LCC. Six consist of a primary, a spectroscopic companion and an astrometric companion. Five quadruple systems are known: two systems consisting of a primary and three visual companions (HIP69113 and HIP81972) and two consisting of a primary, two visual companions and a spectroscopic companion (HIP80112 and HIP78384). HIP77820 is the only quintuple system, consisting of a primary, three visual companions and one spectroscopic companion. The largest known system in Sco OB2 is HIP78374, which contains a primary, four visual companions and two spectroscopic companions.

## 5.2. Binary statistics

The binarity properties of a stellar population are usually quantified in ‘binary fractions’ (e.g., Reipurth & Zinnecker, 1993). Two common definitions in use are the multiple system fraction  $F_M$  and non-single star fraction  $F_{NS}$  (since  $1 - F_{NS}$  is the fraction of stars that is single). Another frequently used quantity is the companion star fraction  $F_C$ <sup>4</sup>, which measures the average number of companion stars per primary star. These quantities are defined as

$$F_M = (B + T + \dots) / (S + B + T + \dots); \quad (6)$$

$$F_{NS} = (2B + 3T + \dots) / (S + 2B + 3T + \dots); \quad (7)$$

$$F_C = (B + 2T + \dots) / (S + B + T + \dots), \quad (8)$$

where  $S$ ,  $B$ , and  $T$  denote the number of single systems, binary systems and triple systems in the association. Table 4 shows several properties of the three subgroups, including the binary statistics that are updated with our new findings.

Figure 15 shows the multiple system fraction  $F_M$  as a function of spectral type of the primary for the three subgroups. For example, 86% of the B0–B3 type *Hipparcos* member stars of UCL have one or more known companion stars. Information

	$D$ (pc)	Age (Myr)	$S$	$B$	$T$	$> 3$	$F_M$	$F_{NS}$	$F_C$
US	145	5–6	63	46	7	3	0.47	0.67	0.61
UCL	140	15–22	131	68	17	4	0.40	0.61	0.52
LCC	118	17–23	112	54	13	0	0.37	0.57	0.45
all			303	171	37	7	0.41	0.61	0.52

**Table 4.** Multiplicity among *Hipparcos* members of Sco OB2. The columns show the subgroup names (Upper Scorpius; Upper Centaurus Lupus; Lower Centaurus Crux), their distances (see de Zeeuw et al., 1999), the ages (de Geus, de Zeeuw, & Lub (1989); Preibisch et al. (2002) for US; Mamajek et al. (2002) for UCL and LCC), the number of known single stars, binary stars, triple systems and  $N > 3$  systems, and the binary statistics (see § 5.2).

about the number of companion stars and the spectral type of the companion stars around the primary is not shown in the figure. The new companion stars found in our AO survey are indicated with the darker shaded parts of the bars. A trend between multiplicity and the spectral type of the primary seems to be present, but this conclusion may well be premature when observational biases are not properly taken into account. Our detection of 41 new close companion stars shows that this is at least partially true: the number of A-type member stars which is in a binary/multiple system in US has doubled as a result of our survey. This strongly supports the statement made in Brown (2001) that the low multiplicity for A- and F-type stars can at least partially be explained by observational biases.

## 6. Conclusions and discussion

We carried out a near-infrared adaptive optics search for companions around 199 (mainly) A and late-B stars in the nearby OB association Sco OB2. Our sample is a selection of the *Hipparcos* membership list of Sco OB2 in de Zeeuw et al. (1999). We find a total of 151 stellar components around the target stars. We use a simple brightness criterion to separate candidate companion stars ( $K_S < 12$  mag) and probable background stars ( $K_S > 12$  mag). The validity of this criterion is verified in several ways (§ 3). Of the detected components, 77 are likely background stars, and 74 are candidate companion stars.

The 74 candidate companions occupy the full range in  $K_S$  magnitude, down to  $K_S = 12$  mag. At the distance of Sco OB2, an M5 main sequence star has a  $K_S$  magnitude of approximately 12 mag. The angular separation between primary and companion ranges from 0.22” to 12.4”. These values correspond to orbital periods of several decades to several thousands of years.

The  $J$ ,  $H$ , and  $K_S$  magnitudes for all observed objects are corrected for distance and interstellar extinction to find the absolute magnitudes  $M_J$ ,  $M_H$ , and  $M_{K_S}$ . The subset of the components with multi-color observations are plotted in a color-magnitude diagram. All (except one) candidate companion stars are positioned close to the 5 Myr (for US) and 20 Myr (for UCL and LCC) isochrones. The background stars are positioned far away from the isochrones.

<sup>4</sup> Note that in Kouwenhoven et al. (2004a,b) we used an incorrect definition of  $F_C$ .

For all observed primaries and companion stars the mass is derived from the absolute magnitude  $M_{K_S}$ . The mass of the A and late-B primaries ranges between  $1.4 M_{\odot}$  and  $7.7 M_{\odot}$  and the mass of their secondaries between  $0.1 M_{\odot}$  and  $3.0 M_{\odot}$ . Most observed companion stars are less massive than their primaries. Most of the systems with previously undocumented companion stars have a mass ratio smaller than 0.25. The mass ratio distribution for the observed objects peaks around  $q = 0.1$  and decreases for higher mass ratios. The minimum and maximum value for the mass ratio of the companion stars that we observed are  $q = 0.022 \pm 0.008$  and  $1.0 \pm 0.34$ . For systems with mass ratio  $q \approx 1$  we cannot say with absolute certainty which is the most massive and therefore the primary star. The mass ratio distribution for binaries with late-B and A type primaries follows the distribution  $f(q) = q^{-\Gamma}$ , with  $\Gamma = 0.33$ . This is similar to the mass ratio distribution observed by Shatsky & Tokovinin (2002) for systems with B type primaries. Relatively few systems with low mass ratio are found, excluding random pairing between primaries and companion stars. The uncertainty in the age of the UCL and LCC subgroups does not effect the mass ratio distribution significantly.

A cross-check with visual, astrometric and spectroscopic binaries in literature shows that 41 of the candidate companion stars are new: 14 in US; 13 in UCL and 14 in LCC. The other 33 candidate companions are already documented in literature. We analyze the presently known data on binarity and multiplicity in Sco OB2, including the 41 new companions that are found in our survey. We conclude that at least 41% of all *Hipparcos* member stars of Sco OB2 are either double or multiple, and we find a companion star fraction  $F_C = 0.52$ . These values are lower limits since the dataset is affected by observational and selection biases.

Our AO observations are close to completeness in the angular separation range  $1'' \lesssim \rho \lesssim 9''$ . Next to the 199 target stars we find 50 companion stars in this angular separation range. This corresponds to an  $F_C$  of 0.25 in this range of angular separation for A and late-B type stars in Sco OB2. This value (not corrected for incompleteness) is slightly higher than the values for B type stars in Sco OB2 ( $F_C = 0.20$  per decade of  $\rho$ ; Shatsky & Tokovinin, 2002) and pre-main sequence stars in Sco OB2 ( $F_C = 0.21$  per decade of  $\rho$ ; Köhler et al., 2000).

At small angular separation ( $\rho \leq 3.75''$ ) no components other than the target stars are detected for magnitudes  $12 \text{ mag} \lesssim K_S \lesssim 14 \text{ mag}$ . This ‘gap’ cannot be explained by observational biases or low-number statistics. A fully populated mass spectrum for the companions (assuming random pairing of binary components from the same underlying IMF) is also incompatible with this gap. This implies a lower limit on the companion masses of  $\sim 0.1 M_{\odot}$ . This is consistent with our finding that the mass ratio distribution points to a deficit of low-mass companions compared to the random pairing case. On the other hand, if we assume that the sources fainter than  $K_S \approx 14 \text{ mag}$  are actually physical companions, a gap may be present in the companion mass distribution. We will carry out follow-up multi-color AO observations to further investigate this issue.

The gap described above might indicate a *brown dwarf desert*, such as observed for solar-type stars in the solar neighbourhood (Duquennoy & Mayor, 1991). The pres-

ence of this gap could support the embryo-ejection formation scenario for brown dwarfs (e.g. Reipurth & Clarke, 2001; Bate, Bonnell, & Bromm, 2003; Kroupa & Bouvier, 2003). This is further supported by the detection of 28 candidate free-floating brown dwarf members of Sco OB2 by Martín et al. (2004).

The observed  $F_M$  decreases with decreasing primary mass. Part of this trend was ascribed by Brown (2001) to observational and selection biases. We lend support to this conclusion with our new AO observations. In particular, the multiplicity fraction for A-type *Hipparcos* members of US is doubled. Nevertheless our knowledge of the present day binary population in Sco OB2 is still rather fragmentary. None of the multiplicity surveys of Sco OB2 so far has been complete due to practical and time constraints, but also because of a lack of full knowledge of the membership of the association. In addition, each observational technique used in these surveys has its own biases. For example, visual binaries are only detected if the angular separation between the components is large enough with respect to the luminosity contrast, which means that with this technique one cannot find the very short-period (spectroscopic) binaries. Moreover the observational biases depend on the way in which a particular survey was carried out (including how background stars were weeded out).

We therefore intend to follow up this observational study by a careful investigation of the effect of selection biases on the interpretation of the results. This will be done through a detailed modeling of evolving OB associations using state-of-the-art N-body techniques coupled with a stellar and binary evolution code. The synthetic OB association will subsequently be ‘observed’ by simulating in detail the various binary surveys that have been carried out. This modeling includes simulated photometry, adaptive optics imaging and *Hipparcos* data, as well as synthetic radial velocity surveys. Examples of this type of approach can be found in Portegies Zwart et al. (2001) (for photometric data) and Quist & Lindegren (2000) (for *Hipparcos* data), where the latter study very clearly demonstrates that an understanding of the observational selection biases much enhances the interpretation of binarity data. Finally, the time dependence of the modeling will also allow us to investigate to what extent stellar/binary evolution and stellar dynamical effects have altered the binary population over the lifetime of the association.

This combination of the data on the binary population in Sco OB2 and a comprehensive modeling of both the association and the observations should result in the most detailed description of the characteristics of the primordial binary population to date.

*Acknowledgements.* We thank Francesco Palla for providing the near-infrared pre-main sequence isochrones and evolutionary tracks. We thank the anonymous referee and Andrei Tokovinin for their constructive criticism, which helped to improve the paper. This research was supported by NWO under project number 614.041.006 and the Leids Kerkhoven Bosscha Fonds.

## References

- Alencar, S. H. P., Melo, C. H. F., Dullemond, C. P., Andersen, J., Batalha, C., Vaz, L. P. R., & Mathieu, R. D. 2003, *A&A*, 409, 1037
- Balega, I. I., Balega, Y. Y., Belkin, I. N., Maximov, A. F., Orlov, V. G., Pluzhnik, E. A., Shkhagosheva, Z. U., & Vasyuk, V. A. 1994, *A&AS*, 105, 503
- Baraffe, I., Chabrier, G., Allard, F., & Hauschildt, P. H. 1998, *A&A*, 337, 403
- Barbier-Brossat, M., Petit, M., & Figon, P. 1994, *A&AS*, 108, 603
- Bate, M. R., Bonnell, I. A., & Bromm, V. 2003, *MNRAS*, 339, 577
- Batten, A. H., Fletcher, J. M., & MacCarthy, D. G. 1997, *VizieR Online Data Catalog*, 5064,
- Bertelli, G., Bressan, A., Chiosi, C., Fagotto, F., & Nasi, E. 1994, *A&AS*, 106, 275
- Beuzit, J.-L. et al. 1997, *Experimental Astronomy*, 7, 285
- Blaauw, A. 1964, *ARA&A*, 2, 213
- Blaauw, A. 1978, *Problems of Physics and Evolution of the Universe*, 101
- Blaauw, A. 1991, in *NATO ASI Ser. C Vol. 342, The Physics of Star Formation and Early Stellar Evolution*, ed C.J. Lada & N.D. Kylafis, (Dordrecht: Kluwer), 125
- van der Blik, N. S., Manfroid, J., & Bouchet, P. 1996, *A&AS*, 119, 547
- Brown, A. G. A., Blaauw, A., Hoogerwerf, R., de Bruijne, J. H. J., de Zeeuw, P. T. 1999, in *NATO ASI Ser. C Vol. 540, The Origin of Stars and Planetary Systems*, ed C.J. Lada & N.D. Kylafis, (Dordrecht: Kluwer), p. 411
- Brown, A. 2001, *Astronomische Nachrichten*, 322, 43
- de Bruijne, J. H. J. 1999, *MNRAS*, 310, 585
- Carpenter, J. M. 2001, *AJ*, 121, 2851
- Carter, B. S. & Meadows, V. S. 1995, *MNRAS*, 276, 734
- Chabrier, G., Baraffe, I., Allard, F., & Hauschildt, P. 2000, *ApJ*, 542, 464
- Couteau, P. 1995, *VizieR Online Data Catalog*, 1209
- Devillard, N. 1997, "The eclipse software", *The Messenger* No 87, 19
- Diolaiti, E., Bendinelli, O., Bonaccini, D., Close, L., Currie, D., & Parmeggiani, G. 2000, *A&AS*, 147, 335
- Dufhot, M., Figon, P., & Meyssonnier, N. 1995, *A&AS*, 114, 269
- Duquenois, A. & Mayor, M. 1991, *A&A*, 248, 485
- ESA 1997, *The Hipparcos and Tycho Catalogues*, ESA SP-1200
- de Geus, E. J., de Zeeuw, P. T., & Lub, J. 1989, *A&A*, 216, 44
- Girardi, L., Bertelli, G., Bressan, A., Chiosi, C., Groenewegen, M. A. T., Marigo, P., Salasnich, B., & Weiss, A. 2002, *A&A*, 391, 195
- Hartkopf, W. I., McAlister, H. A., & Mason, B. D. 2001, *AJ*, 122, 3480
- Hoogerwerf, R. 2000, *MNRAS*, 313, 43
- Hogeveen, S. J. 1990, *Ap&SS*, 173, 315
- Huélamo, N., Brandner, W., Brown, A. G. A., Neuhäuser, R., & Zinnecker, H. 2001, *A&A*, 373, 657
- Hut, P. et al. 2003, *New Astronomy*, 8, 337
- Jordi, C., Ribas, I., Torra, J., & Gimenez, A. 1997, *A&A*, 326, 1044
- Kenyon, S. J. & Hartmann, L. 1995, *ApJS*, 101, 117
- Klessen, R. S., Heitsch, F., & Mac Low, M. 2000, *ApJ*, 535, 887
- Köhler, R., Kunkel, M., Leinert, Ch., Zinnecker, H. 2000, *A&A*, 356, 541
- Kouwenhoven, M. B. N., Brown, A. G. A., Gualandris, A., Kaper, L., Portegies Zwart, S. F., Zinnecker, H. 2004, to appear in proceedings of IAU Coll. 191 'The environments and evolution of binary and multiple stars', held in Mérida, Mexico, 3-7 February 2003, Edited by Allen, C. & Scarfe, C.
- Kouwenhoven, M. B. N., Brown, A. G. A., Zinnecker, H., Kaper, L., Portegies, Zwart, S. F., Gualandris, A. 2004, to appear in the proceedings of the ESO Workshop on 'Science with Adaptive Optics', held in Garching, Germany, 16-19 September 2003, Edited by Brandner, W. & Kasper, M.
- Kraicheva, Z. T., Popova, E. I., Tutukov, A. V., & Yungelson, L. R. 1989, *Nauchnye Informatsii*, 67, 3
- Kroupa, P. 1995a, *MNRAS*, 277, 1492
- Kroupa, P. 1995b, *MNRAS*, 277, 1507
- Kroupa, P. 1995c, *MNRAS*, 277, 1522
- Kroupa, P., Aarseth, S., & Hurley, J. 2001, *MNRAS*, 321, 699
- Kroupa, P. 2002, *Science*, 295, 82
- Kroupa, P. & Boily, C. M. 2002, *MNRAS*, 366, 1188
- Kroupa, P. & Bouvier, J. 2003, *MNRAS*, 346, 369
- Lada, C. J., Lada, E. A. 2003, *ARA&A*, 41, 57
- Larson, R. B. 2001, in *IAU Symp. 200, The Formation of Binary Stars*, ed. H. Zinnecker and R. D. Mathieu (San Francisco: ASP), 93
- Leinert, C., Zinnecker, H., Weitzel, N., Christou, J., Ridgway, S. T., Jameson, R., Haas, M., & Lenzen, R. 1993, *A&A*, 278, 129
- Levato, H., Malaroda, S., Morrell, N., & Solivella, G. 1987, *ApJS*, 64, 487
- Lindroos, K. P. 1985, *A&AS*, 60, 183
- Malkov, O. Y. 1993, *Bulletin d'Information du Centre de Données Stellaires*, 42, 27
- Mamajek, E. E., Meyer, M. R., & Liebert, J. 2002, *AJ*, 124, 1670
- Martín, E. L., Delfosse, X., & Guieu, S. 2004, Accepted for publication in *AJ*
- Mason, B. D. 1995, *VizieR Online Data Catalog*, 610, 70299
- Mathieu, R. D. 1994, *ARA&A*, 32, 465
- Mathis, J. S. 1990, *ARA&A*, 28, 37
- McAlister, H. A., Mason, B. D., Hartkopf, W. I., & Shara, M. M. 1993, *AJ*, 106, 1639
- Miura, N., Baba, N., Ni-Ino, M., Ohtsubo, J., Noguchi, M., & Isobe, S. 1992, *Publications of the National Astronomical Observatory of Japan*, 2, 561
- Palla, F. & Stahler, S. W. 1999, *ApJ*, 525, 772
- Pedoussaut, A., Capdeville, A., Ginestet, N., & Carquillat, J. M. 1996, *VizieR Online Data Catalog*, 4016,
- Portegies Zwart, S. F., McMillan, S. L. W., Hut, P., & Makino, J. 2001, *MNRAS*, 321, 199
- Preibisch, T. & Zinnecker, H. 1999, *AJ*, 117, 2381
- Preibisch, T., Brown, A. G. A., Bridges, T., Guenther, E., & Zinnecker, H. 2002, *AJ*, 124, 404

- Preibisch, T., Stanke, T., & Zinnecker, H. 2003, *A&A*, 409, 147  
 Quist, C.F. & Lindgren, L. 2000, *A&A*, 361, 770  
 Reipurth, B. & Zinnecker, H. 1993, *A&A*, 278, 81  
 Reipurth, B. & Clarke, C. 2001, *AJ*, 122, 432  
 Sartori, M. J., Lépine, J. R. D., & Dias, W. S. 2003, *A&A*, 404, 913  
 Savage, B. D. & Mathis, J. S. 1979, *ARA&A*, 17, 73  
 Shatsky, N. & Tokovinin, A. 2002, *A&A*, 382, 92  
 Sills, A. et al. 2003, *New Astronomy*, 8, 605  
 Sowell, J. R. & Wilson, J. W. 1993, *PASP*, 105, 36  
 Svechnikov, M. A. & Bessonova, L. A. 1984, *Bulletin d'Information du Centre de Données Stellaires*, 26, 99  
 Testi, L., Palla, F., & Natta, A., 1998, *A&AS*, 133, 81  
 Tout, C. A., 1991, *MNRAS*, 250, 701  
 Tokovinin, A. A. 1997, *A&AS*, 124, 75  
 Wolfire, M. G. & Cassinelli, J. P. 1987, *ApJ*, 319, 850  
 Worley, C. E. & Douglass, G. G. 1997, *A&AS*, 125, 523  
 de Zeeuw, T. & Brand, J. 1985, *ASSL Vol. 120: Birth and Evolution of Massive Stars and Stellar Groups*, 95  
 de Zeeuw, P. T., Hoogerwerf, R., de Bruijne, J. H. J., Brown, A. G. A., & Blaauw, A. 1999, *AJ*, 117, 354

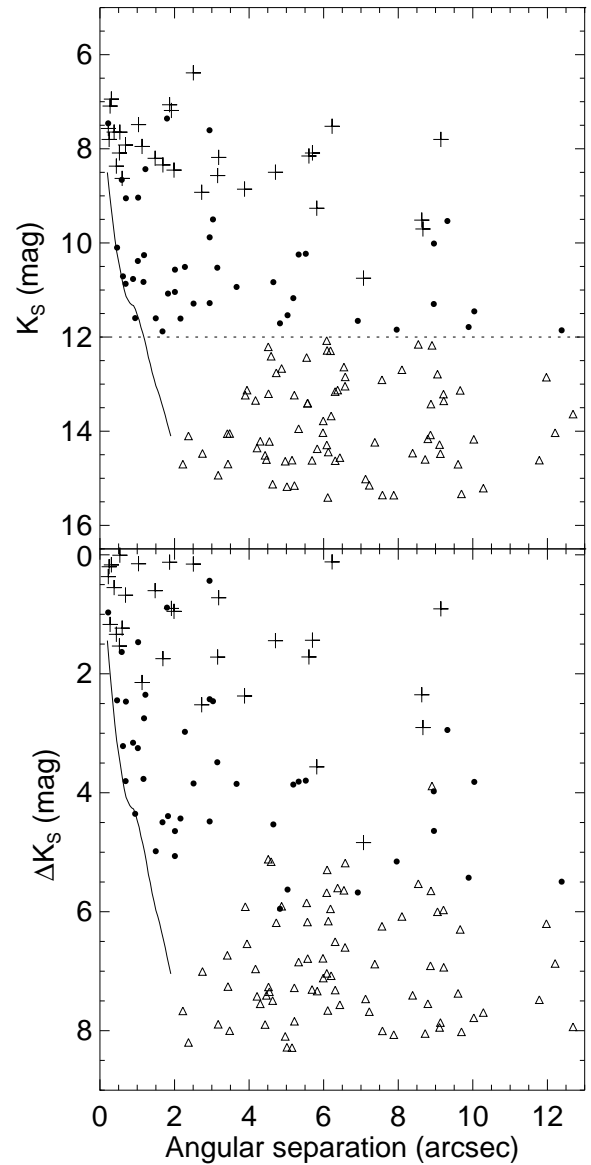


**Fig. 3.** Angular separation between the target stars and observed components as a function of the component's  $K_S$  magnitude (*top*) and component's  $K_S$  magnitude relative to that of the target star (*bottom*). The figures show the 41 new (dots) and 33 previously known (pluses) companion stars ( $K_S < 12$  mag), respectively. The triangles are the 77 background stars ( $K_S > 12$  mag; § 3). The solid curves show the estimated detection limit as a function of angular separation. These figures clearly demonstrate that faint close companions are not detected because of the extended PSF halo of the target star. The effective field of view is  $19.1'' \times 19.1''$ . Companion stars with angular separations larger than  $\frac{1}{2}\sqrt{2} \cdot 19.1'' = 13.5''$  cannot be detected. For small angular separation ( $\rho < 3.5''$ ) no faint ( $K_S > 12$  mag) components are found. This could indicate a gap in the companion mass function, or a lower mass limit for companion stars at small separation (see § 4.3).

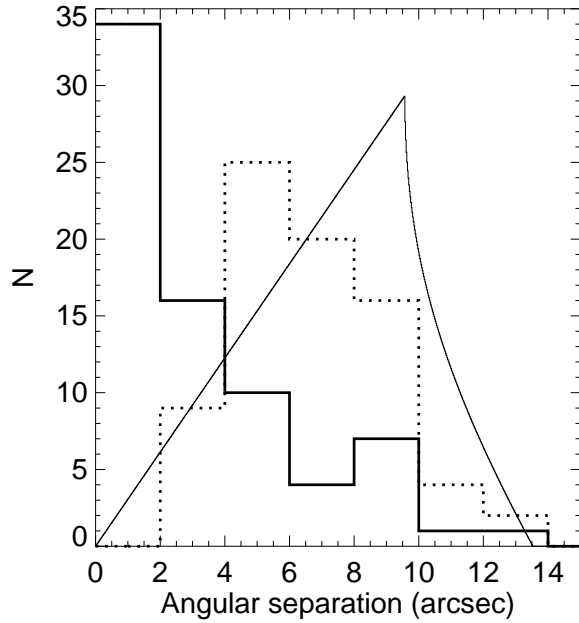


**Fig. 4.** The number of objects per angular separation bin versus angular separation (bin size  $2''$ ). The distribution of presumed background stars (dotted histogram) is clearly different from that of the companion stars (solid histogram). The expected angular separation distribution for background stars (in units of stars per bin size) is represented with the solid curve. The curve is normalized such that the number of stars corresponds to the expected number of background stars with  $12 \text{ mag} < K_S < 16 \text{ mag}$  (cf. Figure 5). The excess of close ( $\rho \lesssim 6''$ ) companions could be caused by faint companion stars that are misclassified as background stars. Objects with  $\rho < 0.1''$  are too deep in the PSF halo of the primary to be detectable. Objects with  $\rho > 15''$  cannot be measured due to the limited field of view of the ADONIS/SHARPII+ system.

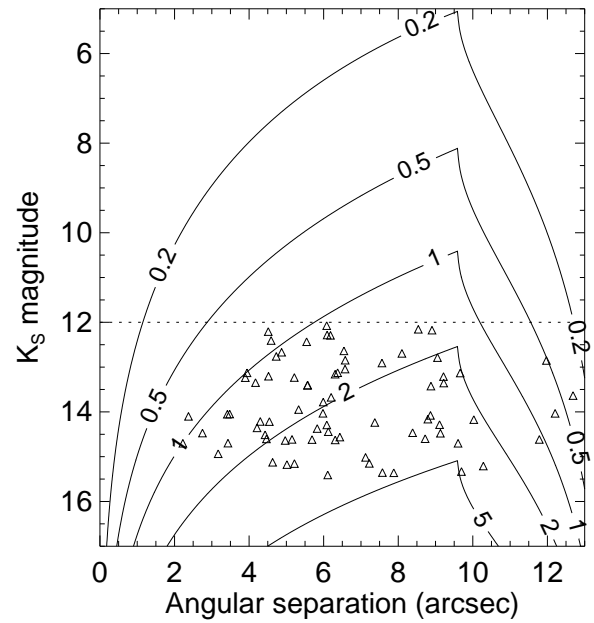


**Fig. 5.** The expected background star distribution as a function of angular separation and the  $K_S$  magnitude distribution of background stars as observed by Shatsky & Tokovinin (2002). The distribution of background stars over the field of view is assumed to be homogeneous. The triangles represent the observed stellar objects that we classify as background stars. The contours indicate the background star density in units of  $\text{arcsec}^{-1} \text{mag}^{-1}$ . The distribution is normalized, so that for  $14 \text{ mag} \leq K_S \leq 15 \text{ mag}$  and  $5'' \leq \rho \leq 13''$  the number of background stars equals 19, i.e. the observed number of background stars with these properties. Observational biases are not considered. The dashed line represents our criterion to separate companion stars ( $K_S \leq 12 \text{ mag}$ ) and background stars ( $K_S > 12 \text{ mag}$ ). The excess of background stars at small angular separations could be caused by faint companion stars that are misclassified as background stars.

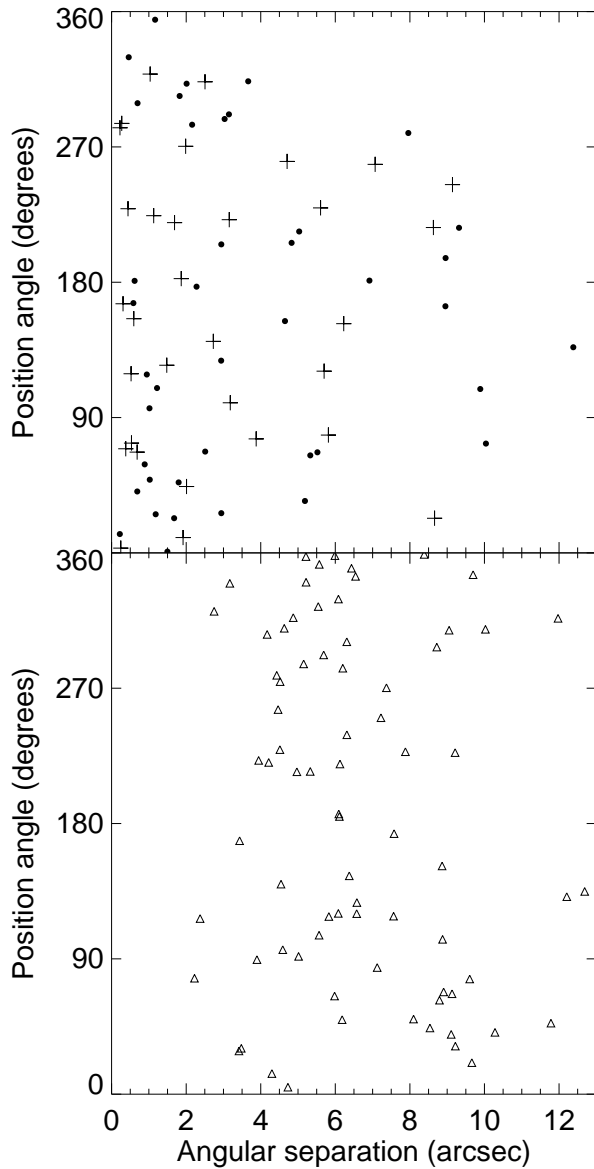


**Fig. 6.** *Top:* the distribution of presumed companion stars over angular separation and position angle. Previously known companions and new companions are indicated with the pluses and dots, respectively. *Bottom:* the distribution of background stars over angular separation and position angle. The distribution of companion stars and background stars over position angle is random for angular separation smaller than  $9.6''$  (see text). The companion stars are more centrally concentrated than the background stars.

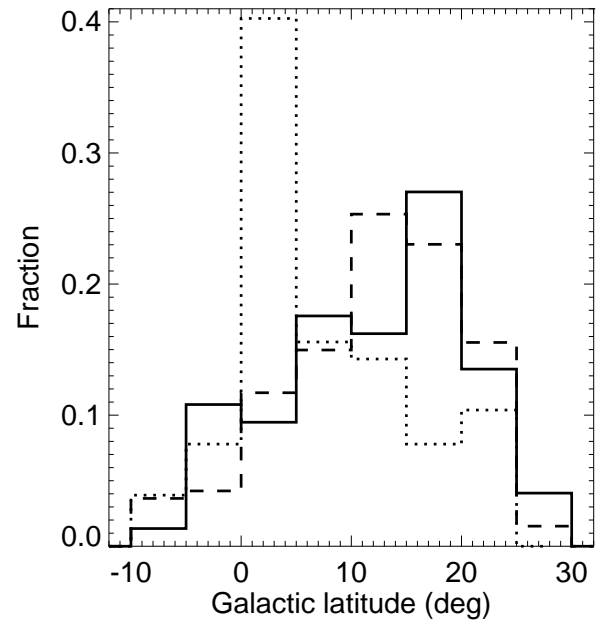


**Fig. 8.** The distribution of the 74 detected candidate companion stars (solid histogram) and 77 presumed background stars (dotted histogram) as a function of Galactic latitude. The dashed histogram represents the distribution of *Hipparcos* member stars over Galactic latitude. The bin size is  $5^\circ$  for the three histograms. The distributions are clearly different: the companion star and *Hipparcos* member star distribution peak at about the central Sco OB2 latitude. As expected, the background star distribution peaks at the location of the Galactic plane.

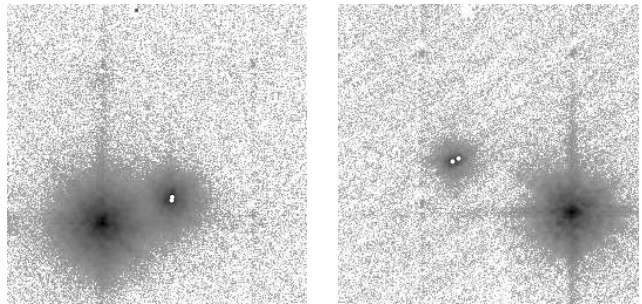


**Fig. 9.** *Left:* The hierarchical triple HIP68532. Both companion stars (indicated with the white dots) were previously undocumented. *Right:* HIP69113, another multiple system, where both close companion stars (white dots) were previously undocumented. A third known companion star with angular separation of  $28''$  is not detected in our survey because of the large angular separation.

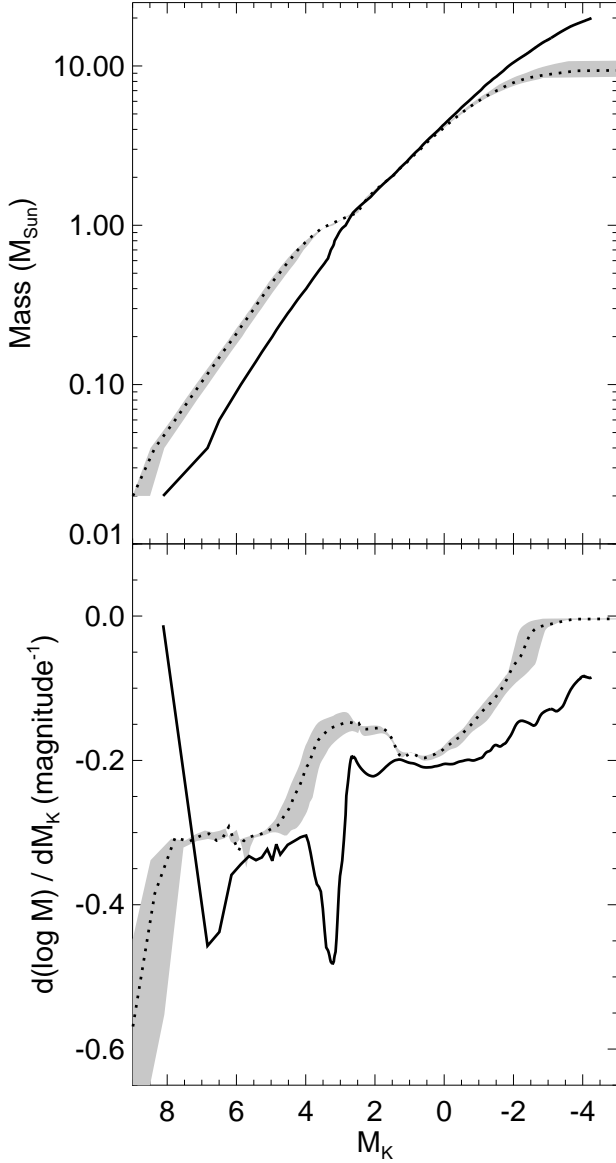


**Fig. 11.** *Top:* The relation between mass and  $M_{K_S}$  magnitude. The 5 Myr isochrone (solid curve) is used to find masses of the companion stars in US, while the 20 Myr isochrone (dotted curve) is used for the UCL and LCC subgroups. The gray-shaded area is enclosed by the 15 Myr and 23 Myr isochrones, and represents the uncertainty in the age of the UCL and LCC subgroups. For objects at the mean Sco OB2 distance of 130 pc,  $M_{K_S} = 6$  corresponds to  $K_S = 11.6$ . *Bottom:* The derivative of the mass-magnitude relation. The conversion from  $M_{K_S}$  to mass is most accurate where the absolute value of the derivative  $dM/dM_{K_S}$  is small.

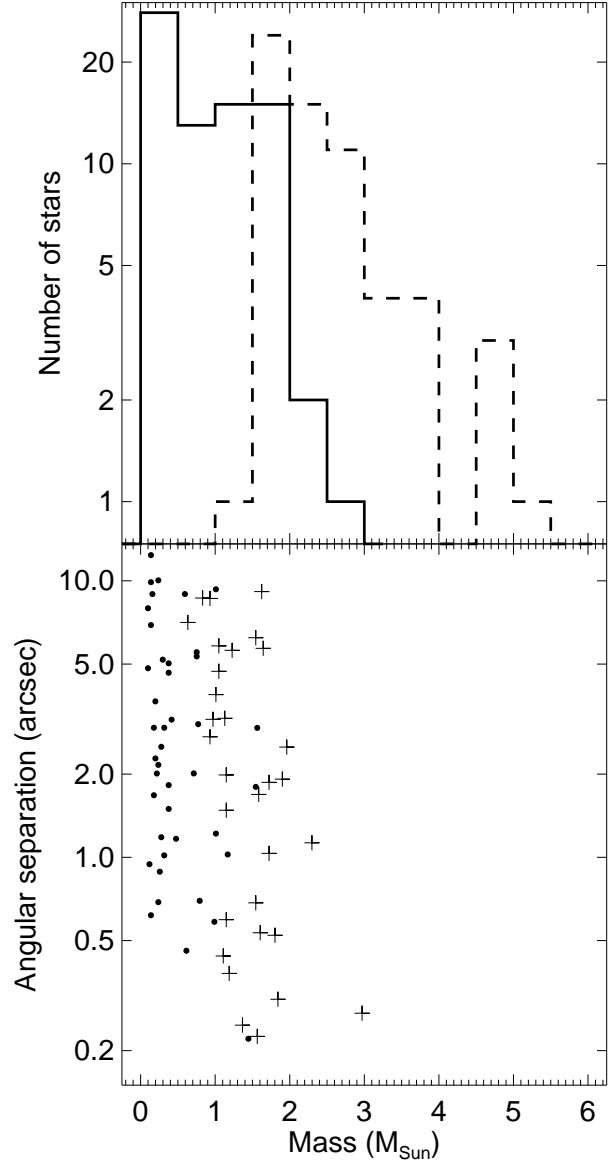


**Fig. 12.** *Top:* The mass distribution of the 74 companion stars (solid histogram) and corresponding primaries (dashed histogram) observed in our AO survey. The bin size is  $0.5 M_{\odot}$ . Masses are derived from their  $K_S$  magnitude and age (see § 4.3). The median errors in the mass are  $0.4 M_{\odot}$  for the primaries and  $0.1 M_{\odot}$  for the companions. *Bottom:* Companion star mass versus angular separation. New and previously known companion stars are indicated as dots and pluses, respectively. Low-mass close companion stars are not detected due to the PSF wings of the corresponding primary star.

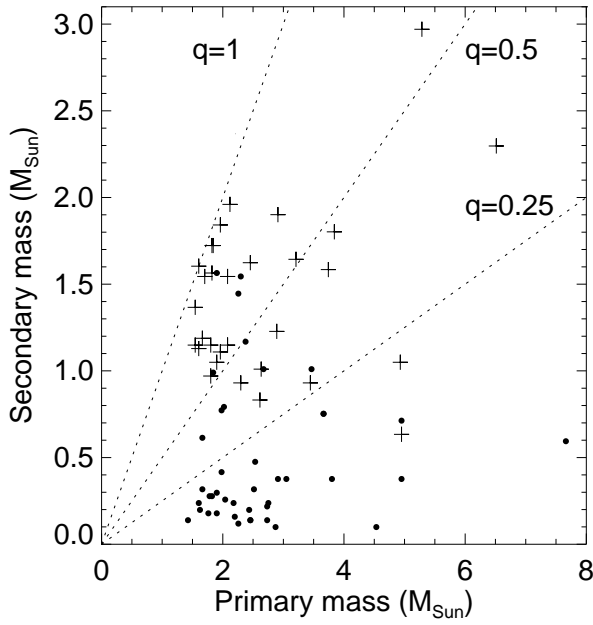


**Fig. 13.** Companion star mass versus primary star mass. The dashed lines represent the  $q = 0.25$ ,  $q = 0.5$ , and  $q = 1$  binaries and are shown to guide the eye. The 41 new companion stars and the 33 previously known companion stars are indicated with dots and pluses, respectively. The observed companion stars have masses lower than their associated primaries. Most systems with previously undocumented companion stars have  $q < 0.25$ .

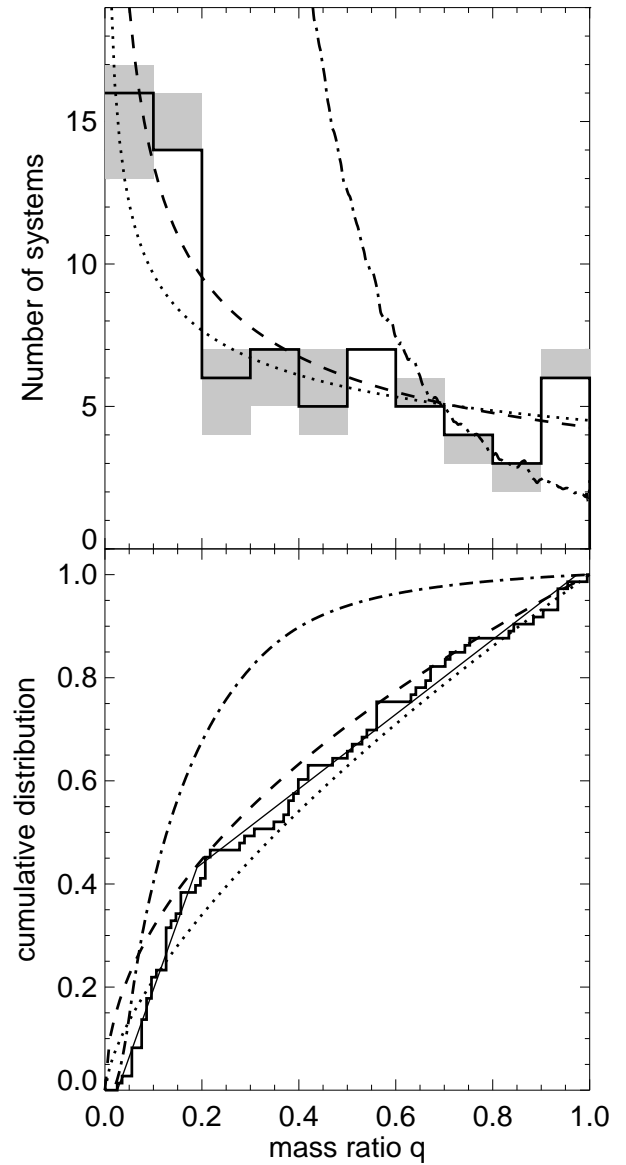


**Fig. 14.** *Top:* The mass ratio distribution for the 74 systems for which we observe companion stars in our near-infrared AO survey (histogram). The mass ratio is defined as  $q = M_c/M_p$  where  $M_c$  is the companion star mass and  $M_p$  the mass of the corresponding primary star. All primaries are *Hipparcos* member stars with A and late-B spectral type. The  $q$  distribution does not change significantly if ages of 15 Myr or 23 Myr for UCL and LCC are assumed (gray-shaded areas). The mass ratio distributions  $f(q) = q^{-\Gamma}$  are represented by the curves. For our observations we find  $\Gamma = 0.33$  (dotted curve). Shatsky & Tokovinin (2002) find  $\Gamma = 0.5$  (dashed curve). The distribution which follows from random pairing (dash-dotted curve) is clearly excluded. The curves are normalized using the observed mass ratio distribution for the companion stars in the range  $0.5 < q < 1.0$ . *Bottom:* The observed cumulative mass ratio distribution (histogram). The dotted and dashed curve are cumulative distribution functions corresponding to  $\Gamma = 0.33$  and  $\Gamma = 0.5$ , respectively. The fitted function described in Equation 4 is shown as the thin solid curve. The dash-dotted curve represents the cumulative  $q$  distribution for random pairing.

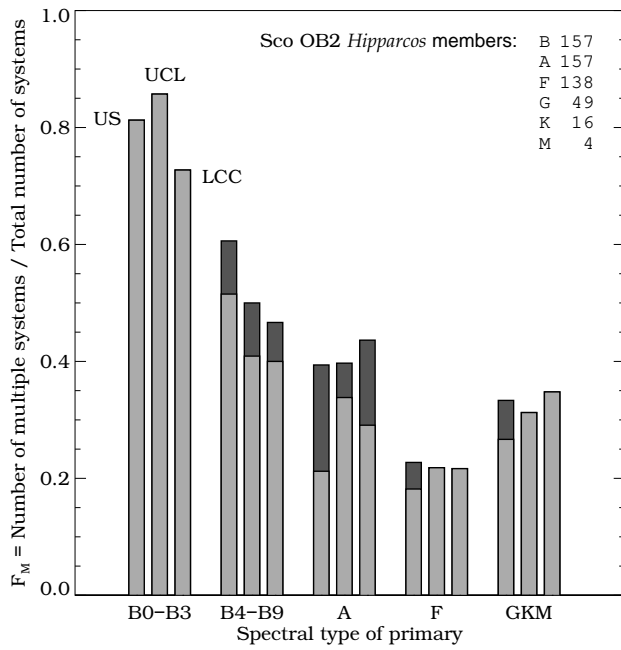


**Fig. 15.** The fraction of stellar systems which is multiple versus the spectral type of the primary, for the three subgroups of Sco OB2. Only confirmed Hipparcos member primaries are considered here. The binarity dataset consists of literature data and our near-infrared AO survey. The light and dark grey parts of the bars correspond to literature data and the new data presented in this article, respectively. The spectral types of the companion stars (not included in this plot) are always later than those of the primary stars. Apparently, the multiplicity is a function of spectral type, but this conclusion may well be premature when observational biases are not properly taken into account. That this is at least partly true, is supported by our detection of 41 new close companion stars at later spectral types.

# Online Material

Table .1:

Star	<i>J</i> mag	<i>H</i> mag	<i>K<sub>S</sub></i> mag	type	$\rho$ (")	<i>PA</i> (°)	stat	group	remarks
HIP50520			6.23	A1V			p	LCC	
			6.39		2.51	313.3	c		
HIP52357			7.64	A3IV			p	LCC	
			7.65		0.53	73.0	c		
			11.45		10.04	72.7	nc		
HIP53524			6.76	A8III			p	LCC	
			12.67		4.87	316.9	b		
HIP53701	6.30	6.37	6.48	B8IV			p	LCC	
	9.05	8.76	8.86		3.88	75.8	c		
	13.06	12.93	13.04		6.57	120.1	b		
HIP54231			6.75	A0V			p	LCC	
HIP55188			7.43	A2V			p	LCC	
HIP55899			7.07	A0V			p	LCC	
HIP56354			5.78	A9V			p	LCC	
HIP56379			5.27	B9Vne			p	LCC	
HIP56963			7.46	A3V			p	LCC	
HIP56993			7.38	A0V			p	LCC	
			11.88		1.68	23.1	nc		
HIP57809			6.61	A0V			p	LCC	
HIP58416			7.03	A7V			p	LCC	
			8.66		0.58	166.1	nc		
HIP58452			6.51	B8/B9V			p	LCC	
HIP58465			6.32	A2V			p	LCC	
HIP58720			6.05	B9V			p	LCC	
HIP58859			6.52	B9V			p	LCC	
HIP59282			7.00	A3V			p	LCC	
HIP59397			7.01	A2V			p	LCC	
HIP59413			7.46	A6V			p	LCC	
			8.18		3.18	99.8	c		
			15.15		7.22	250.3	b		
HIP59502			6.80	A2V			p	LCC	
			11.28		2.94	26.4	nc		
			12.79		9.05	308.6	b		
HIP59898			5.99	A0V			p	LCC	
HIP60084			7.65	A1V			p	LCC	
			10.10		0.46	329.6	nc		
HIP60183			6.33	B9V			p	LCC	
HIP60561			6.59	A0V			p	LCC	
HIP60851			5.98	A0Vn			p	LCC	
			11.04		2.01	44.1	nc		
			11.66		6.92	181.1	nc		
HIP61257			6.60	B9V			p	LCC	
			12.43		5.54	324.3	b		
HIP61265			7.44	A2V			p	LCC	
			11.29		2.51	67.4	nc		
			14.70		3.43	168.6	b		
HIP61639			6.94	A1/A2V			p	LCC	
			7.06		1.87	182.4	c		
			14.36		4.21	220.6	b		
HIP61782			7.56	A0V			p	LCC	
HIP61796			6.37	B8V			p	LCC	
			11.79		9.89	109.0	nc		
			11.86		12.38	136.8	nc		

	13.35		4.17	305.8	b	
HIP62002	7.09	A1V			p	LCC
	7.65		0.38	69.2	c	
	13.95		5.33	214.6	b	
HIP62026	6.49	B9V			p	LCC
	7.46		0.22	12.5	nc	
HIP62058	6.17	B9Vn			p	LCC
HIP62179	7.20	A0IV/V			p	LCC
	7.57		0.23	282.7	c	
	14.03		12.21	131.3	b	
	14.60		4.47	255.8	b	
HIP63204	6.47	A0p			p	LCC
	7.36		1.80	46.9	nc	
HIP63236	6.66	A2IV/V			p	LCC
	12.91		7.56	118.4	b	
	12.85		11.97	316.5	b	
HIP63839	6.66	A0V			p	LCC
	13.78		5.99	358.1	b	
	14.21		4.30	13.7	b	
	13.16		6.31	300.9	b	
HIP64320	6.22	Ap			p	LCC
HIP64515	6.78	B9V			p	LCC
	6.94		0.31	165.7	c	
HIP64892	6.82	B9V			p	LCC
HIP64925	6.88	A0V			p	LCC
HIP64933	6.29	A0V			p	LCC
HIP65021	7.26	B9V			p	LCC
HIP65089	7.37	A7/A8V			p	LCC
HIP65178	6.71	B9V			p	LCC
HIP65219	6.52	A3/A4III/IV			p	LCC
HIP65394	7.25	A1Vn...			p	LCC
HIP65426	6.78	A2V			p	LCC
HIP65822	6.68	A1V			p	LCC
	11.08		1.82	303.9	nc	
HIP65965	7.51	B9V			p	LCC
	15.21		10.28	41.1	b	
HIP66068	7.04	A1/A2V			p	LCC
HIP66447	7.16	A3IV/V			p	UCL
HIP66454	6.33	B8V			p	LCC
HIP66566	7.36	A1V			p	LCC
HIP66651	7.35	B9.5V			p	LCC
	15.36		7.58	173.3	b	
HIP66722	6.32	A0V			p	UCL
HIP66908	6.86	A4V			p	UCL
HIP67036	6.69	A0p			p	LCC
HIP67260	7.03	A0V			p	LCC
	8.37		0.44	228.9	c	
	14.70		2.22	77.1	b	
HIP67919	6.58	A9V			p	LCC
	9.05		0.70	299.1	nc	
HIP68080	6.28	A1V			p	UCL
	7.19		1.92	10.2	c	
HIP68532	7.03	A3IV/V			p	UCL
	9.50		3.03	288.6	nc	
	10.53		3.15	291.7	nc	
HIP68781	7.38	A2V			p	UCL

HIP68867			7.17	A0V			p	UCL
			11.61		2.16	284.8	nc	
HIP68958			6.72	Ap...			p	UCL
HIP69113	6.25	6.32	6.43	B9V			p	UCL
	11.14	10.51	10.25		5.33	64.8	nc	
	11.19	10.46	10.23		5.52	66.9	nc	
HIP69749			6.62	B9IV			p	UCL
			11.60		1.50	0.8	nc	
			12.69		8.10	50.0	b	
			13.40		5.57	352.4	b	
			14.16		8.79	62.5	b	
			14.48		9.13	66.8	b	
			14.51		4.43	278.6	b	
HIP69845			7.78	B9V			p	UCL
HIP70441			7.31	A1V			p	UCL
HIP70455			7.07	B8V			p	UCL
HIP70626			6.56	B9V			p	UCL
HIP70690			7.71	B9V			p	UCL
HIP70697			7.17	A0V			p	UCL
HIP70809			6.54	Ap...			p	UCL
			14.64		4.97	214.4	b	
			14.60		8.72	297.3	b	
HIP70904			6.39	A6V			p	UCL
			12.08		6.08	120.3	b	
			14.17		10.03	309.2	b	
HIP70918			6.35	A0/A1V			p	UCL
HIP70998			7.06	A1V			p	UCL
			10.83		1.17	354.6	nc	
HIP71140			7.13	A7/A8IV			p	UCL
HIP71271			7.57	A0V			p	UCL
HIP71321			7.17	A9V			p	UCL
HIP71724			6.79	B8/B9V			p	UCL
			9.70		8.66	23.0	c	
HIP71727			6.89	A0p			p	UCL
			7.80		9.14	245.0	c	
HIP72140			7.09	A1IV/V			p	UCL
			12.21		4.51	229.1	b	
HIP72192	6.71	6.71	6.71	A0V			p	UCL
HIP72627	6.54	6.54	6.53	A2V			p	UCL
HIP72940			6.85	A1V			p	UCL
			8.57		3.16	221.6	c	
HIP72984			7.05	A0/A1V			p	UCL
			14.37		5.83	118.1	b	
			8.50		4.71	260.3	c	
HIP73145			7.54	A2IV			p	UCL
HIP73266			7.30	B9V			p	UCL
HIP73341			6.67	B8V			p	UCL
HIP73393			7.21	A0V			p	UCL
HIP73937			6.05	Ap			p	UCL
			14.05		3.48	30.5	b	
HIP74066			6.08	B8IV			p	UCL
			8.43		1.22	109.6	nc	
HIP74100			6.12	B7V			p	UCL
HIP74479			6.31	B8V			p	UCL
			10.83		4.65	154.1	nc	

HIP74657			6.97	B9IV				p	UCL
HIP74752			6.84	B9V				p	UCL
			13.13			9.66	21.0	b	
HIP74797			7.55	A2IV				p	UCL
HIP74985			7.53	A0V				p	UCL
			13.13			6.37	145.2	b	
HIP75056			7.31	A2V				p	UCL
			11.17			5.19	34.5	nc	
HIP75077			6.97	A1V				p	UCL
HIP75151			6.65	A+...				p	UCL
			8.09			5.70	120.9	c	
HIP75210			6.82	B8/B9V				p	UCL
HIP75476			6.88	A1/A2V				p	UCL
HIP75509			7.40	A2V				p	UCL
HIP75647			5.86	B5V				p	UCL
HIP75915			6.44	B9V				p	UCL
			8.15			5.60	229.4	c	
HIP75957			7.24	A0V				p	UCL
			13.41			5.56	105.7	b	
			13.21			9.21	227.1	b	
HIP76001			7.60	A2/A3V				p	UCL
			7.80			0.25	3.2	c	
			8.20			1.48	124.8	c	
			12.85			6.58	127.5	b	
HIP76048			6.26	B6/B7V				p	UCL
HIP76071	7.05	7.10	7.06	B9V				p	US
		11.28	10.87			0.69	40.8	nc	
HIP76310			7.35	A0V				p	US
HIP76503			6.25	B9IV				p	US
HIP76633			7.51	B9V				p	US
HIP77150			7.28	A2V				p	UCL
HIP77295			7.64	A2IV/V				p	UCL
			15.13			4.63	309.9	b	
HIP77315			7.24	A0V				p	UCL
			7.92			0.68	67.0	c	
HIP77317			7.37	B9.5V				p	UCL
			14.24			37.37	137.3	p	UCL
						32.78	146.8	b	
HIP77457			7.33	A7IV				p	US
HIP77523			7.41	B9V				p	UCL
HIP77858			5.40	B5V				p	US
HIP77859			5.57	B2V				p	US
HIP77900			6.44	B7V				p	US
HIP77909			6.19	B8III/IV				p	US
HIP77911	6.67	6.71	6.68	B9V				p	US
	12.68	12.20	11.84			7.96	279.3	nc	
HIP77939			6.56	B2/B3V				p	US
			8.09			0.52	119.1	c	
HIP77968			7.00	B8V				p	UCL
			12.64			6.54	344.4	b	
			14.56			6.43	349.8	b	
HIP78099			7.35	A0V				p	US
HIP78168			5.91	B3V				p	US
HIP78196			7.08	A0V				p	US
HIP78246			5.84	B5V				p	US
HIP78494			7.11	A2m...				p	US
HIP78530	6.87	6.92	6.87	B9V				p	US

		14.56	14.22		4.54	139.7	b	
HIP78533			6.99	Ap			p	UCL
			12.28		6.09	186.3	b	
HIP78541			6.99	A0V			p	UCL
HIP78549			7.13	B9.5V			p	US
			14.62		11.78	47.3	b	
HIP78663			7.76	F5V			p	US
			13.42		8.88	103.0	b	
			15.41		6.11	184.7	b	
HIP78702			7.41	B9V			p	US
HIP78754			6.95	B8/B9V			p	UCL
HIP78756			7.16	Ap			p	UCL
			9.52		8.63	216.4	c	
HIP78809	7.41	7.50	7.51	B9V			p	US
	11.08	10.45	10.26		1.18	25.7	nc	
HIP78847			7.32	A0V			p	US
			11.30		8.95	164.0	nc	
HIP78853			7.50	A5V			p	UCL
			8.45		1.99	270.4	c	
			15.02		7.12	84.2	b	
HIP78877			6.08	B8V			p	US
HIP78956	7.52	7.54	7.57	B9.5V			p	US
	9.76	9.12	9.04		1.02	48.7	nc	
HIP78968	7.40	7.41	7.47	B9V			p	US
		14.59	14.47		2.75	321.1	b	
HIP78996			7.46	A9V			p	US
HIP79031			7.00	B8IV/V			p	US
HIP79044			6.91	B9V			p	UCL
			15.18		5.02	91.6	b	
HIP79098			5.90	B9V			p	US
			14.10		2.37	116.8	b	
HIP79124	7.16	7.14	7.13	A0V			p	US
	11.38	10.55	10.38		1.02	96.2	nc	
HIP79156	7.56	7.56	7.61	A0V			p	US
	11.62	10.89	10.77		0.89	58.9	nc	
HIP79250			7.49	A3III/IV			p	US
			10.71		0.62	180.9	nc	
HIP79366			7.47	A3V			p	US
HIP79410			7.05	B9V			p	US
			14.93		3.17	339.8	b	
HIP79439			6.97	B9V			p	US
HIP79530			6.60	B6IV			p	US
			8.34		1.69	219.7	c	
HIP79599			6.30	B9V			p	US
HIP79622			6.34	B8V			p	US
HIP79631			7.17	B9.5V			p	UCL
			7.61		2.94	127.9	nc	
			14.08		8.86	151.8	b	
HIP79739			7.24	B8V			p	US
			11.60		0.94	118.6	nc	
HIP79771			7.09	B9V			p	US
			10.94		3.66	313.6	nc	
HIP79785			6.41	B9V			p	US
HIP79860			7.88	A0V			p	US
HIP79878			7.06	A0V			p	US
HIP79897			6.99	B9V			p	US

HIP80019			7.08	A0V				p	US		
HIP80024			6.73	B9II/III				p	US		
HIP80059			7.44	A7III/IV				p	US		
HIP80126			6.44	B6/B7Vn				p	US		
HIP80142			6.60	B7V				p	UCL		
			12.16			8.54	44.0	b			
			9.53			9.32	216.2	c			
HIP80238	7.45	7.45	7.34	A1III/IV				p	US		
	7.96	7.66	7.49			1.03	318.5	c			
HIP80324			7.33	A0V+...				p	US		
			7.52			6.23	152.5	c			
HIP80371			6.40	B5III				p	US		
			8.92			2.73	140.6	c			
			13.36			9.22	32.0	b			
HIP80425			7.40	A1V				p	US		
			8.63			0.60	155.8	c			
HIP80461			5.92	B3/B4V				p	US		
			7.09			0.27	285.6	c			
HIP80474	6.13	6.08	5.76	A				p	US	JH	
	13.00	12.30	11.71			4.83	206.2	nc		JH	
HIP80493			7.05	B9V				p	US		
HIP80591			7.82	A5V				p	UCL		
HIP80799	7.68	7.75	7.46	A2V				p	US	JH	
	10.94	10.35	9.88			2.94	205.2	nc		JH	
HIP80896			7.53	F3V				p	US		
			10.51			2.28	177.0	nc			
HIP80897			7.78	A0V				p	UCL		
HIP81136			5.21	A7/A8+...				p	UCL		
HIP81316			6.72	B9V				p	UCL		
HIP81472			5.96	B2.5IV				p	UCL		
			13.23			5.21	357.5	b			
			13.20			4.52	274.4	b			
HIP81474			5.74	B9.5IV				p	US		
HIP81624			5.80	A1V				p	US		
			7.95			1.13	224.3	c			
HIP81751			8.29	A9V				p	UCL		
			12.18			8.91	68.0	b			
			14.44			6.12	219.6	b			
HIP81914			6.34	B6/B7V				p	UCL		
			12.29			6.18	49.5	b			
			14.28			9.11	39.8	b			
			14.61			5.15	286.2	b			
HIP81949			7.32	A3V				p	UCL		
			13.23			3.90	89.5	b			
			14.05			3.42	28.7	b			
			14.70			9.60	76.6	b			
			14.63			6.31	239.0	b			
			14.62			5.69	292.2	b			
			15.15			5.22	340.5	b			
			15.33			9.70	345.5	b			
HIP81972			5.92	B3V				p	UCL		
			10.57			2.01	312.0	nc			
			10.75			7.07	258.4	c			
			11.54			5.03	213.7	nc			
HIP82154	6.89	7.22	7.05	B9IV/V				p	UCL	JH	
	14.86	14.93	14.47			8.39	359.0	b		JH	

HIP82397			7.28	A3V				p	US	
			15.36			7.88	227.7	b		
HIP82430			7.25	B9V				p	UCL	
			12.41			4.59	96.1	b		
			14.03			5.98	65.3	b		
			14.29			6.08	329.3	b		
HIP82560	6.83	6.97	6.58	A0V				p	UCL	JH
		13.86	12.76			4.73	4.6	b		H
		14.40	13.13			3.94	222.0	b		H
		14.38	13.68			6.20	283.3	b		H
HIP83457			6.49	A9V				p	UCL	
HIP83542			5.38	G8/K0III				p	US	
			10.01			8.96	196.1	nc		
HIP83693			5.69	A2IV				p	UCL	
			9.26			5.82	78.4	c		
			13.64			12.69	134.9	b		